COUPLING OF A SEMICONDUCTOR LASER

TO A SINGLE-MODE FIBER

Nu Yu
B.S., Huazhong University, Wuhan, China, 1982

A thesis submitted to the faculty
of the Oregon Graduate Center
in partial fulfillment of the
requirements for the degree
Master of Science
in
Electrical Engineering

February, 1987

The thesis "Coupling of a Semiconductor Laser to a Single-mode fiber" by Nu Yu has been examined and approved by the following Examination Committee:

Dae M. Kim, Thesis Research Advisor
Professor
Department of Applied Physics and Electrical Engineering
Oregon Graduate Center

J. Fred Holmes
Professor and Chairman
Department of Applied Physics and Electrical Engineering
Oregon Graduate Center

Richard K. DeFreez
Assistant Professor
Department of Electrical Engineering
Portland State University

Tom Hawkins
Principal Scientist
Electronic Systems Laboratory
Tektronix, Inc.

ACKNOWLEDGMENTS

I would like to gratefully acknowledge all of the people who have made this thesis possible.

Dr. Dae M. Kim, my advisor, in particular is owed a debt of gratitude for his guidance, understanding, patience, and financial support along the way. I also thank Judy L. Passman, one of the collaborators of this project, for the discussions regarding the microlens fabrication and experiment data.

I would like to thank Dr. Richard K. DeFreez for his many helpful suggestions and efforts to improve this thesis. I am also very thankful to Drs. J. Fred Holmes and Tom Hawkins for their participation on my thesis examination committee and their very careful examination of this thesis. Thanks are due the Department of Applied Physics and Electrical Engineering for the use of the computer facilities during this work.

Finally, I am most indebted to my parents for their encouragement and expectation, and also to my wife Yuan for her support.

DEDICATION

To my parents and Uncle Siyao for their love and support.

Table of Contents

List of Figures

List of Tables

ABSTRACT

COUPLING OF A SEMICONDUCTOR LASER TO A SINGLE-MODE FIBER

Nu Yu, M.S.

Oregon Graduate Center, 1987

Supervising Professor: Dae M. Kim

The efficient coupling between a semiconductor laser and a single-mode fiber is a key element for fully utilizing the single-mode fiber for the optical communication. In this thesis, the Gaussian beam approach is used for analyzing the coupling of a single-mode laser diode to a single-mode optical fiber by a microlens. Two analytical methods based on both the *ABCD* law and the diffraction theory are presented. The effect of a microlens on both the phase and amplitude of a Gaussian beam are discussed in detail. The presented analysis specifies the optimum coupling in terms of laser and fiber parameters and the laser to fiber distance. Furthermore, the coupling efficiencies achievable in hemispheric and etched conical microlenses systems are explicitly compared. The present analysis shows that an coupling efficiency as high as 62% is achievable with the optimal choice of laser and fiber parameters. Additionally, theoretically obtained coupling efficiency are compared with the experimental data for both butt and etched fibers.

1. INTRODUCTION

Optical fiber transmission technology has developed rapidly due to improvements in fabrication of optical fibers, light sources, and other optical devices. This technology can be divided into two categories according to the type of fibers used. The first is the multimode fiber transmission system, i.e., medium-capacity short-haul transmission system (SH system)[1]. The second is the single-mode fiber (SMF) transmission system, i.e., large-capacity long-haul transmission system (LH system)[1]. Fully engineered telecommunication traffic-carrying systems of multimode fibers have already been in operation for several years. The large core diameter of multimode fibers makes it easier to couple optical power into such fibers and makes the alignment for splices less critical than for single-mode fibers. The coupling losses in multimode systems are sufficiently low that more efforts to further reduce their values are no longer justified. Multimode systems have the advantage that they can be used with light emitting diode sources which are less expensive and less complex than laser diodes required for a single-mode system. However, they are only suitable for short distance transmission or low bandwidth applications because of the limitations on their transmission capacity imposed by the intrinsic intermodal group delay difference[2].

With the advent of semiconductor laser diodes (LD) operating in longer wavelength region of 1 ~ 1.8 μm, optical fiber transmission using single-mode

fibers (SMF) becomes feasible. Owing to low fiber loss in that spectral region and to wide-band single-mode fiber characteristics over the multimode system, the single-mode system is especially attractive for high capacity, long-haul communication systems and submarine communication systems[2-5]. Research emphasis has been focused on single-mode fiber systems using this long wavelength region[6-11]. Furthermore, the transmission loss of single-mode fiber drops below 1 dB/km, and fiber chromatic dispersion approaches zero near 1.3 μm wavelength[7,12]. Its superior light guiding characteristics over multimode fibers results in a significant increase in repeater spacing for transmission systems. This increase also brings about an improvement in system reliability and economy as well as maintenance convenience.

Results of transmission experiments have shown that the repeater spacing, even in high data rate systems, is limited mainly by fiber transmission loss and coupling loss between semiconductor lasers and single-mode fibers[9,13]. Recently, the transmission loss of single-mode fibers has been reduced to values as low as 0.4 dB/km at 1.3 μm and 0.2 dB/km at 1.55 μm for single-mode fibers[14,15]. Therefore, reduction of coupling loss to obtain a highly efficient power coupling between a semiconductor laser diode and a single-mode fiber is important in order to fully utilize the single-mode fiber for the optical communication.

There are a number of factors which cause the coupling loss to be high. The core diameter of a single-mode fiber is about 5 ~ 10 μm and as small as one-tenth that of a multimode fiber. Typically, the light beam emanating from the rectangular aperture on a laser diode may diverge much more rapidly perpendicular to the junction plane than it does parallel to the junction plane. The laser-

light power that can be launched into the single-mode fiber by using the simple butt coupling method is small, with typical loss of the order of 7 ~ 11 dB[8, 16], because of mismatch of the semiconductor laser and single-mode fiber modal profiles (spot sizes). Moreover, the beam output from diode laser with a strip geometry generally has an elliptical cross section while the HE_{11} fiber mode has a circular shape. For high coupling efficiency, the elliptical laser diode mode must be transformed to match that of the circular single-mode fiber. Hence, efficient coupling elements, such as lenses, between laser diodes and single-mode fibers are the key devices in optical communication systems[15].

Usually a precise alignment of laser, lens, and single-mode fiber is required to reduce the coupling loss. The alignment requirements are slightly relaxed when a self-centered lens (i.e., a microlens) with its base equal to the core's cross section is fabricated on the end surface of the fiber either by etching or by photolithography. This technique also shows that maximum coupling is obtained when the laser-fiber separation is finite, thereby avoiding the need to bring the two into physical contact. The etched conical end method is rather attractive in that the alignment between lens and core is inherently built into the system[15], and it is also suitable for batch processing. Eisenstein *et al.* reported a theoretical analysis with initial experimental results[17]. They have measured the coupling efficiency of the conical lens and interpreted the results using the thin-lens approximation. Their consideration of the conical lens as only a phase shifter, however, excludes the effect of the conical lens on the amplitude of a Gaussian beam. This thesis presents an analysis for coupling a semiconductor laser to a single-mode optical fiber and describes the microlens characteristics. Because the

effect of the microlens on the amplitude of a Gaussian beam is an important term that can not be neglected, the effects on both the phase and the amplitude are considered. Furthermore, the theoretical treatment is developed by introducing the diffraction theory for investigating the diffraction effect of the microlens. The purpose of the analysis is to

1. establish the optimum coupling scheme such as the microlens shape and the separation between a laser and a fiber for a given laser;

2. estimate the maximum coupling efficiency from a coupling scheme;

3. evaluate the diffraction effect of the microlens; and

4. compare the diffraction theory with conventional method of the *ABCD* law for the applicability and the exactitude.

The organization of the thesis is as follows. Chapter 2 presents an overview of problems, and the methods for coupling a semiconductor laser to an optical fiber. Section 2.1 gives a general description of the optical coupling problem. Section 2.2 details the development of previous methods used for improving coupling efficiency.

The Gaussian beam approach is used to analyze the coupling of a single-mode laser diode to a single-mode fiber in Chapter 3. Section 3.1 presents the Gaussian approximation of the radiation emanating from the single-mode laser diode. Section 3.2 describes the transformation of the Gaussian beam by an optical system using the *ABCD* law. Section 3.3 discusses a Gaussian approximation of the mode of the single-mode fiber. The formulation of the coupling efficiency is presented in Section 3.4.

Chapter 4 further develops the theory to actually compute the coupling efficiencies for the case of microlenses. Sections 4.2 and 4.3 discuss the conical microlens and the hemispherical microlens, respectively.

In Chapter 5, the diffraction theory is used to evaluate the laser field after a hemispherical microlens. The Dirichlet boundary-value problem of the Helmholtz wave equation is solved with a Green function. Section 5.1 specifies the field immediately inside the microlens surface by means of the vector form of the field and the electromagnetic boundary conditions at interface between different media. In Section 5.2, an analysis based on the generalized Helmholtz-Kirchhoff's diffraction formula is derived. Section 5.3 gives the Dirichlet Green function associated with the Dirichlet boundary-value problem to obtain the integral presentation of the solution. Section 5.4 evaluates the field at the base of the microlens. In Section 5.5, the results are compared with those using the *ABCD* law.

Chapter 6 presents the methods for fabricating microlenses and compares theoretically calculated efficiency values with experimental results. Section 6.1 describes the fabrication of the microlens using an etching method. In Section 6.2, the calculated values of the coupling loss are compared with experimental results for the specific case of a buried heterostructure InGaAsP semiconductor laser to a single-mode fiber, both with and without an etched conical microlens.

Concluding remarks are made in Chapter 7.

2. OVERVIEW OF LASER-TO-FIBER COUPLING

A practical high-bit-rate and long-distance optical fiber communication system using single-mode fibers requires both a rigid connection and a highly efficient coupling between the laser and the fiber. The first requirement makes the device easy to handle, rugged, and reliable. The second requirement has been a very important factor in reducing the total losses of single-mode fiber transmission systems. Because butt joint between the laser and the fiber provides poor coupling efficiency, various coupling methods have been suggested. In this chapter, the coupling problem is addressed and the various coupling techniques are discussed and compared.

2.1 Coupling Problems between Lasers and Fibers

A general configuration of laser-to-fiber coupling is illustrated in Figure 2.1. The principle of such coupling scheme can be summarized as follows: The laser spot size, i.e., the beam waist, has to be matched to the fiber spot size with respect to phase and amplitude distributions. The phase condition is met when imaging the parallel wave front of the laser beam waist onto the parallel wave front of the fiber beam waist. The amplitude condition requires, in most cases, a transformation of the elliptical laser beam waist into a circular fiber beam waist,

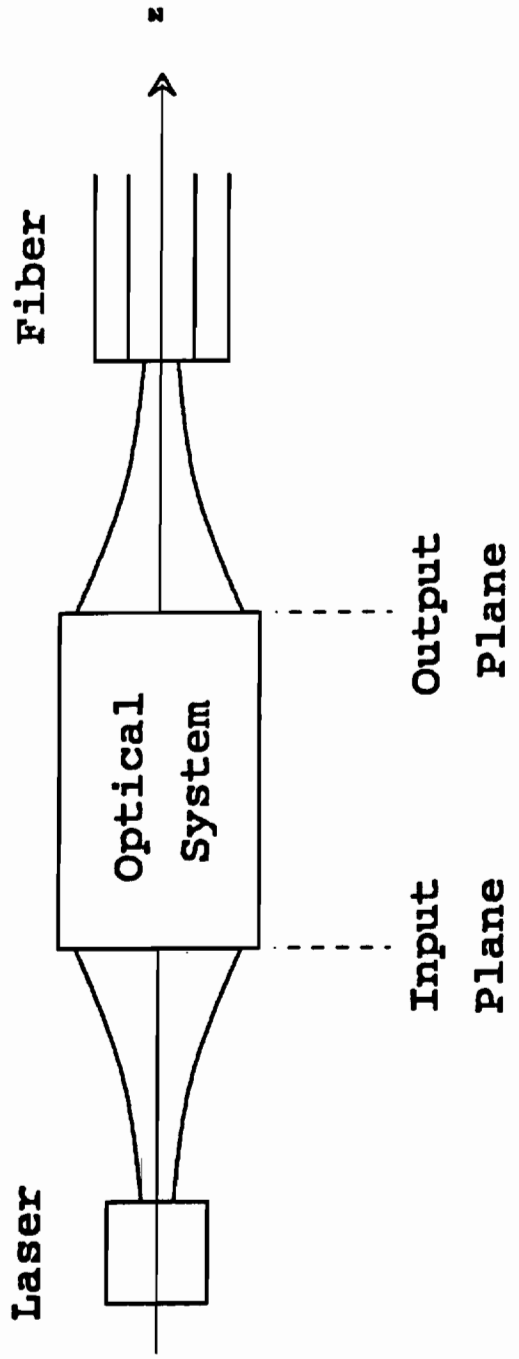

Figure 2.1 Coupling of a semiconductor laser to a fiber through a optical system.

matching the sizes and amplitude distributions, respectively. To obtain these transformations, an optical system has to be employed. The basic problem is to calculate the power-coupling efficiency between the laser and the optical fiber through the optical system, which may consist of lenses and other elements. The optical system converts the diverging laser beam into a converging beam at the fiber end surface, and a certain fraction of the optical power is coupled into the fiber. In order to analyze and understand the coupling process, it is desirable to specify the power-coupling efficiency in terms of the position and characteristics of the fiber and the parameters of the optical system.

Although the problem of laser-to-fiber coupling efficiency is similar in many respects to the classical optical imaging problem, there is an important difference. This difference is that the laser diode, lens, and the optical fiber comprise together a coherent system, rather than an incoherent system with a Lambertian source as is most often encountered in classical optics. This means that field distributions and the coherent optical transfer function are of primary concern, rather than irradiance distributions and incoherent optical transfer function.

In principle, it is possible to make a lossless passive component that will provide nearly perfect coupling to the optical fiber provided that the laser radiates into a single spatial mode of the radiation field. However, it is not possible to provide lossless coupling to a single-mode fiber if the laser radiates into more than one mode, or even if the laser always radiates into a single mode but not always into the same spatial mode.

The overall coupling efficiency may be analyzed in a series of steps that correspond to determining the field distributions of the light at various planes in

the optical system. Naturally, the field distribution on the plane of the laser output facet is closely related to the mode pattern of the laser. From the laser field, diffraction theory can be used on a general ground to determine the field at any plane that is the input plane of the optical system.

The field distribution at a second such plane, the output plane of the optical system, is then determined as a transformation of the input field distribution of the optical system. The transformation is governed by the properties of the optical system. For large optical systems where the paraxial approximation condition is satisfied, the transformation can be described by the paraxial imaging properties of the optical system and by the coherent optical transfer function, a multiplicative term that describes the imperfections, or aberrations, of the optical system.

The output field distribution of the optical system produces a so-called image field distribution, which again can be calculated by diffraction theory, at the image plane located at the endface of the fiber. The power coupling efficiency is then the squared modulus of the field normalized overlap integral of the image field distribution and the mode pattern of the fiber. For computational purposes, the overlap integral can be transformed to any convenient plane in the optical system.

Conceptually, this description of the coupling efficiency is convenient because it allows one to follow the propagation of light through the optical system from the laser to the fiber. The overlap integral thus expressed in the output plane of the optical system most easily provides insight into the coupling efficiency problem, and is also most convenient for coupling efficiency

calculations. This methodology is capable of presenting a clear and simple understanding of how various imperfections will affect the coupling efficiency.

2.2 Methods for Improving Coupling Efficiency

The basic and practical requirements for coupling schemes are (i) low coupling loss, (ii) small size and small number of components, (iii) easy fabrication, and (iv) easy handling. It would be desirable to couple directly the power from the laser diode into the fiber via a small air gap spacing without any additional optical components. Although this scheme is relatively simple and fairly tolerant of lateral offsets of the fiber, the optical power coupling efficiencies obtained are fairly small, e.g., efficiencies measured were about 8% for a single-mode fiber[18]. The reason for such low value is, as stated in Chapter 1, that the distributions of the electric field of the semiconductor laser and the fiber are very different. In 1972 Cohen of Bell Laboratories suggested[18] a method of attaching a hemicylindrical lens onto a fiber tip to increase the coupling efficiency. The hemicylindrical lens was designed such as to collimate the laser beam perpendicular to the junction plane in order to transform its cross section from a elliptic shape to a circular shape. The coupling efficiencies were improved to 23% for single-mode fibers and 40% for multimode fibers, respectively[18]. In practice, however, such a small lens is difficult to fabricate and attach. During the past decade, many efforts have been devoted to improving the laser-to-fiber coupling, and various novel types of coupling have been developed. As a result, the coupling efficiency has been enhanced to more than 50% for single-mode fibers[19] and more than 90% for multimode fibers in laboratories. These coupling methods can be divided

into three categories: (i) single lens coupling, (ii) confocal lenses coupling, and (iii) microlens coupling (see Figure 2.2).

2.2.1 Single Lens Coupling

The method utilizes a separated single lens such as cylindrical or ball lens. It was in 1975 when Weidel proposed a device using one cylindrical lens between a laser and a single-mode fiber[20]. The lens was an unclad transparent cylindrical fiber of small diameter with its axis in the plane of the laser junction and normal to the fiber. With a suitable choice of diameter and refractive index for the fiber lens, and by choosing the best laser-fiber separation, the light beam behind the lens was partially collimated to have a nearly circular cross-section. Even though this method did not lead much improvement of the coupling efficiency due to a low numerical aperture and spherical aberrations of the lenses and had serious mounting and alignment problems, many attempts have been stimulated, since then, to improve this coupling scheme. Theoretical and experimental studies using selfoc lens[21], gradient-index-rod lens[22], ball lens[23,24], cylindrical lens[25], and GRIN-rod lens[23] etc., have been reported. Coupling loss of as low as 1.0 dB was obtained recently using a planoconvex, high-numerical-aperture GRIN-rod lens[26]. The marked low coupling loss was obtained by realizing an extremely small lens wave front aberration. Although high coupling efficiency can be achieved using this method, it imposes stringent alignment tolerance due to very small lenses used. One has to perfectly align the laser with the lens as well as the lens with the fiber for the low loss coupling to be obtained. Alternatively, confocal lensing schemes, discussed next, have also been used.

- **BUTT COUPLING — POOR COUPLING**

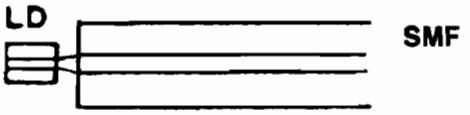

- **METHODS FOR IMPROVING COUPING**

1. **SINGLE LENS COUPLING**

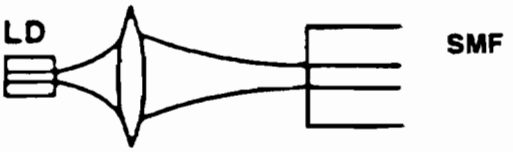

2. **CONFOCAL LENSES COUPLING**

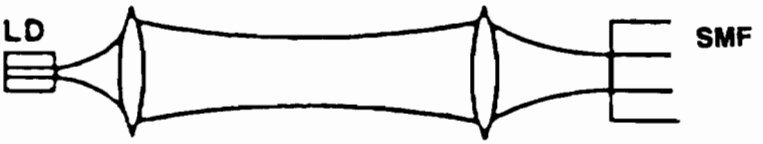

3. **MICROLENS COUPLING**

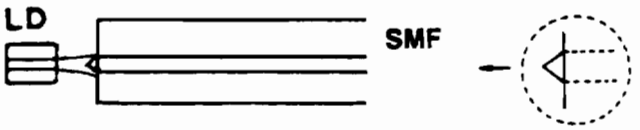

Figure 2.2 Coupling methods for a laser diode to a single-mode fiber.

2.2.2 Confocal Lenses Coupling

The second group consists of a confocal two-lens approach, where two relatively large lenses are positioned in nearly confocal condition[19,27,28,29]. This method results in good coupling efficiency, large longitudinal offset tolerances for the lenses, and the possibility of producing a hermetic package without using fiber seals. Coupling loss of 3.0 dB has been obtained[19,30]. If the fiber tolerances could be expanded to the level similar to those for multimode fiber, ease of laser diode module fabrication could be markedly improved. This method, however, suffers from several severe drawbacks: (i) The alignment of this system is more difficult than the single lens system because of more lenses are used. (ii) Several individual components have to be fixed in position once they are aligned. (iii) The laser performance is disturbed by reflections not only from the lenses front surfaces but also from the lenses back surfaces and from the fiber input flat.

2.2.3 Microlens Coupling

The microlens technique is based on the fabrication of a very small lens of the same size as the fiber cross section and extremely short focal length on the fiber itself. Thus it can avoid the several drawbacks mentioned above. In 1973, Kato proposed[31] a coupling method with a hemispherical fiber end formed by thermal melting. The acceptance angle of the fiber was increased markably by such a simple tapered fiber end, and a coupling efficiency of more than 50% was evaluated by Kato. The tapered hemispherical fiber end is attractive since it combines a variety of features such as simple fabrication, a reasonable coupling

efficiency and a reduced influence on reflected lights. However, there is a number of drawbacks in this approach, which are inherent in the fabrication method. The lens at the top of the taper is formed by surface tension of the head end, and consists, therefore, of the fiber material itself. Furthermore, these tapers are long in comparison with the fiber diameter, which results in an increased sensitivity to deformation. Finally, the lens can only be reproduced by careful control of the heating and drawing conditions. After Kato's initial work, Cohen[32], Weidel[33], and Timmermann[34] successively developed this method by forming a sufficiently small lens directly on the fiber endface, which is called a microlens. using a variety of procedures including photoresist exposure[35], etching[33] and combination of etching and melting[34] techniques. The lens can transform the beam emanating from the junction laser into a beam that more closely matches the circular HE_{11} fiber mode. This method significantly improved the coupling efficiency between semiconductor lasers and single-mode fibers to 23% for a fiber with a hemispherical microlens, 34% with a hemicylindrical microlens[35], 40% with a cylindrical microlens, and more than 50% with an etched conical lens[17,36], as well as 80% for a multimode fiber[34]. Although these microlenses cannot be fabricated easily, the alignment problem can be greatly relaxed since they are self-centered, or, automatically adjusted to the core of the fiber, which is obviously an important feature. High coupling efficiency can also be obtained when this method is used in optimal coupling conditions.

Table 2.1 summarizes some of the experimental work together with the reported lowest coupling loss for the single-mode fiber.

Table 2.1 Various Methods of Laser-Diode-to-Fiber Coupling Together with the Corresponding Observed Coupling Loss

Method	Laser[λ(μm)]	Coupling Loss (dB)	Year	Reference
Photolithographic	GaAs[0.9]	4.7-6.4	1974	[35]
Cylindrical lens	GaAs	3	1979	[25]
Hemispherical tipped lens	InGaAsP[1.29]	2.5-2.9	1980,'80,'85	[37, 38, 39]
Hemispherical taper end	InGaAsP[1.29]	≤4.56	1980	[40]
Confocal lenses	InGaAsP[1.29]	3.5	1980	[28]
Confocal lenses	InGaAsP[1.29]	3	1985	[19]
Etched conical lens	GaAlAs	4.56	1981	[41]
Etched conical lens	InGaAsP[1.3]	2.84-3	1982	[17]
Etched conical lens	InGaAsP[1.3]	3.1	1986	[36]

To further improve the laser-to-fiber coupling efficiency, a better understanding of the optical coupling phenomenon is required. In this work, the research emphasis is put on the theoretical treatment. A Gaussian beam approach is presented and used to analyze the coupling process in the following chapters.

3. GAUSSIAN BEAM APPROACH FOR COUPLING

In order to calculate the efficiency of coupling a laser diode to a single-mode fiber, it is necessary to determine a model for the radiation field of the laser diode. A Gaussian beam approximation will be employed to describe the laser diode mode. When this mode is launched into an optical fiber, a set of modes of the fiber can be excited. However, a given single-mode fiber can only support the HE_{11} mode which will also be approximated by a Gaussian distribution. A theory for coupling between two Gaussian beams will be developed to compute the coupling efficiency of a single-mode laser diode to a single-mode fiber.

3.1 Gaussian Approximation of the Laser Radiation Field

Single-mode laser diodes are essential to the achievement of loss-limited transmission distances in optical fiber communication systems. The most widely encountered type of laser beam in optics is one where the intensity distribution at planes normal to the propagation direction is Gaussian[42]. The radiation field patterns of gallium arsenide junction lasers have been reported in the literature as closely approximating Hermite-Gaussian beam profiles, both parallel and perpendicular to the junction plane[43-45]. Most laser diodes have an active region

that has a large width-to-height ratio. Their radiation field can be approximated by a two-dimensional Gaussian beam, i.e., an elliptical Gaussian beam with a very wide beam width along the junction plane[46].

The present analysis treats a single-mode laser diode emitting a fundamental transverse mode. Figure 3.1 shows a Gaussian beam as it focuses down to its waist and diverges to the right. The wave front emitted by a gain-guided diode laser has astigmatism[47]. When gain guiding predominates in the junction plane, the beam waist parallel to the junction plane is a virtual source and is displaced a virtual distance behind the laser output facet[48]. At the same time, the waist perpendicular to the junction plane remain at the mirror because of index guiding in this plane. Usually, index-guided lasers such as buried-heterostructure lasers have little astigmatism effect, i.e., the virtual distance is very small within a couple of microns[49]. The present analysis neglects astigmatism, so that the beam waist is taken to be situated at the laser output facet. To describe the field distribution, a complex amplitude ψ and a Cartesian (x,y,z) coordinate system are used. The x and y coordinates are perpendicular and parallel to the junction plane, respectively, while the positive z axis is chosen so that the radiation emanating from the laser output facet propagates into the half-space $z>0$. A bar will be used to denote quantities referring to the outgoing light wave (emerging from the surface of the laser at the left). The Gaussian field emanated from a rectangular aperture on a laser diode is described by[18]

$$\bar{\psi}_s = \left(\frac{2}{\pi}\frac{1}{\bar{w}_x \bar{w}_y}\right)^{\frac{1}{2}} \exp\left[-x^2\left(\frac{1}{\bar{w}_x^2}+\frac{ik}{2\bar{R}_x}\right)-y^2\left(\frac{1}{\bar{w}_y^2}+\frac{ik}{2\bar{R}_y}\right)\right], \qquad (3.1)$$

where $k = 2\pi/\lambda$, is the propagation constant in free space, and λ is the free-space

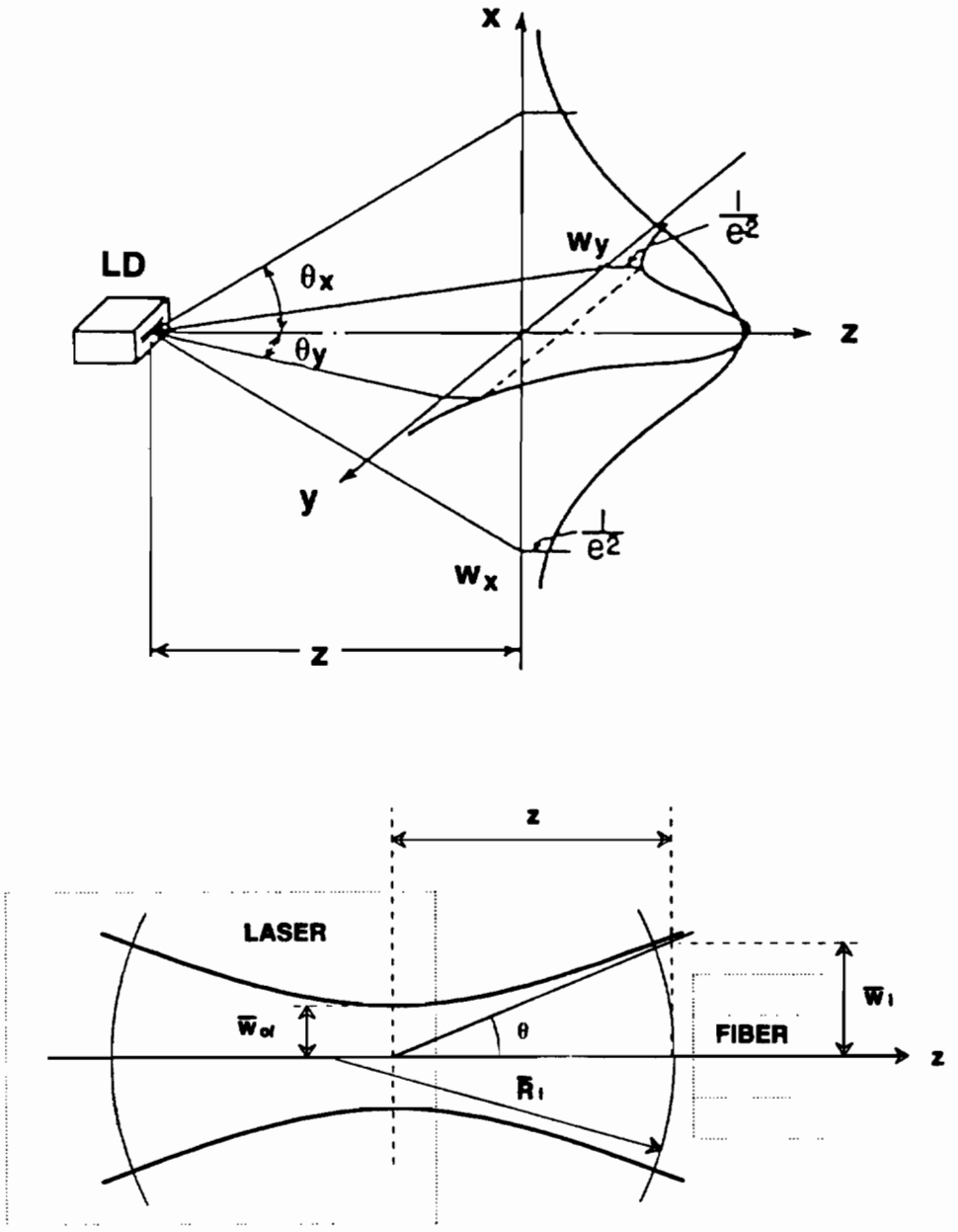

Figure 3.1 Parametrization of a Gaussian beam.

wavelength emitted. The beam parameters at a convenient reference plane separated by distance, z, from the laser surface are the beam spot sizes $\bar{w}_x$, $\bar{w}_y$ perpendicular and parallel to the laser's junction plane and the wavefront radii of curvature $\bar{R}_x$,$\bar{R}_y$ perpendicular and parallel to the junction plane. The beam spot sizes are the beam waist radii defined at $1/e^2$ points of the emitted optical power in the transverse direction.

For the sake of brevity, we take l to denote the x and y directions. The laser beam is characterized by its minimum beam radius $\bar{w}_{ol}$ and the location of the beam waist. The parameters $\bar{w}_l$ and $\bar{R}_l$ that specify a Gaussian beam completely at a reference plane may be written in terms of their values ($\bar{w}_l = \bar{w}_{ol}$, $\bar{R}_l = \infty$) at the surface of the laser, $z = 0$. As the light beam propagates in space it expands due to diffraction, but the transverse field distribution remains Gaussian. The law of expansion is[50]

$$\bar{w}_l = \bar{w}_{ol}\left[1+\left(\frac{\lambda z}{\pi\,\bar{w}_{ol}^2}\right)^2\right]^{1/2}. \tag{3.2}$$

We can define the angle of the far-field beam divergence at $1/e^2$ of the maximum intensity distribution by the equation

$$\theta_{1/e} = \frac{2\lambda}{\pi\,\bar{w}_{ol}}. \tag{3.3}$$

This is a rigorous manifestation of wave diffraction[42], according to which a wave that is confined in the transverse direction to an aperture of radius $\bar{w}_{ol}$ will spread (diffract) in the far field ($z >> \pi\bar{w}_{ol}^2/\lambda$) according to Equation (3.3). In order to obtain the angle $\theta_{1/2}$ for full width at half maximum (FWHM) of the far-field intensity distribution, a factor of $(ln2\,/\,2)^{1/2}$ should be multiplied in Equation

(3.3), yielding

$$\theta_{1/2} = \sqrt{2\,ln\,2}\,\frac{\lambda}{\pi\,\bar{w}_{ol}} \,. \tag{3.4}$$

The radius of the phase front curvature changes along the optic axis according to the law[50]

$$\bar{R}_l = z\left[1+\left(\frac{\pi\,\bar{w}_{ol}^2}{\lambda z}\right)^2\right] . \tag{3.5}$$

It is convenient to combine the beam parameters $\bar{\omega}_l$ and $\bar{R}_l$ in a complex-valued parameter $\bar{q}_l$ defined by

$$\frac{1}{\bar{q}_l} = \frac{1}{\bar{R}_l} - i\,\frac{\lambda}{\pi\,\bar{w}_l^2} \,. \tag{3.6}$$

The propagation and transformation laws for this beam parameter are particularly simple and allow one to trace Gaussian beams through more complicated optical structures. The parameters $\bar{R}_l$ and $\bar{w}_l$ can, of course, be recovered from the real and imaginary parts of $1/\bar{q}_l$. One can obtain the parameter $\bar{q}_l$ in a different form

$$\bar{q}_l = z + i\,\frac{\pi\,\bar{w}_{ol}^2}{\lambda} = z + i\,\bar{z}_{ol} \,, \tag{3.7}$$

where the parameter

$$\bar{z}_{ol} = \frac{\pi\,\bar{w}_{ol}^2}{\lambda} \tag{3.8}$$

is the confocal beam parameter which is the distance from the waist in which the beam spot size increases by $2^{1/2}$ and is a convenient measure of the convergence of

the beam. The smaller $\bar{z}_{ol}$, the "stronger" the convergence. At the origin, $z = 0$, the radius of wave front curvature at the waist plane is infinite and the beam reaches its minimum radius $\bar{w}_{ol}$. Thus we have a very simple expression for the complex beam parameter at the beam waist

$$\bar{q}_{ol} = i\,\bar{z}_{ol} \,. \tag{3.9}$$

3.2 Transformation of Gaussian Beam

Since the mode parameters of both laser and fiber will not match, in general, one normally inserts suitable optical elements into the path of the beam to maximize the matching for optimum coupling, as indicated in Figure 2.1. When a Gaussian beam passes paraxially through optical elements a new beam waist is formed, and the parameters in the expansion laws are changed. The paraxial transformation of a Gaussian beam by an optical system is conveniently described by the $ABCD$ law[51,52]. This law also allows a "black box" approach to the study of optical modes. Given an optical system which is charactered by the elements A, B, C and D of the ray matrix, the input $\bar{q}_{ol}$ parameter is transformed into the output q_l parameter according to

$$q_l = \frac{A\,\bar{q}_{ol} + B}{C\,\bar{q}_{ol} + D} \,. \tag{3.10}$$

Using Equation (3.9) we can write the reciprocal of q_l parameter as

$$\begin{aligned} \frac{1}{q_l} &= \frac{C\,\bar{q}_{ol} + D}{A\,\bar{q}_{ol} + B} = \frac{i\,\bar{z}_{ol}\,C + D}{i\,\bar{z}_{ol}\,A + B} \\ &= \frac{BD + \bar{z}_{ol}^2\,AC}{(\bar{z}_{ol}\,A)^2 + B^2} - i\,\frac{(AD - BC)\,\bar{z}_{ol}}{(\bar{z}_{ol}\,A)^2 + B^2} \,. \end{aligned} \tag{3.11}$$

Comparing the real and imaginary parts, respectively, of this equation with those of

$$\frac{1}{q_l} = \frac{1}{R_l} - i\frac{\lambda}{\pi w_l^2}, \tag{3.12}$$

we obtain the spot size ω_l and radius of curvature R_l of the output beam as

$$\omega_l = \frac{\lambda}{\pi \bar{w}_{ol}}\left[\frac{(\pi \bar{w}_{ol}^2 A / \lambda)^2 + B^2}{AD - BC}\right]^{\frac{1}{2}}, \tag{3.13}$$

$$R_l = \frac{(\pi \bar{w}_{ol}^2 A / \lambda)^2 + B^2}{BD + (\pi \bar{w}_{ol}^2 / \lambda)^2 AC}. \tag{3.14}$$

Once transformation matrices are found, one can specify the output q_l parameter in terms of known input $\bar{q}_{ol}$ parameter. The determinant of the transformation matrix is unity, that is

$$\det \begin{pmatrix} A & B \\ C & D \end{pmatrix} = AD - BC = 1. \tag{3.15}$$

Since the determinant of the product of matrices is equal to the product of determinants of the corresponding matrices, this holds for any cascade. Equations (3.13) and (3.14) can thus be rewritten as

$$w_l = \frac{\lambda}{\pi \bar{w}_{ol}}\left[\left(\frac{\pi \bar{w}_{ol}^2}{\lambda} A\right)^2 + B^2\right]^{\frac{1}{2}}, \tag{3.16}$$

$$R_l = \left(\frac{\pi \bar{w}_{ol} w_l}{\lambda}\right)^2 \left[BD + \left(\frac{\pi \bar{w}_{ol}^2}{\lambda}\right)^2 AC\right]^{-1}. \tag{3.17}$$

Hence the field distribution of the laser diode at the reference plane is expressed

as

$$\psi_s = \left(\frac{2}{\pi}\frac{1}{w_x w_y}\right)^{\frac{1}{2}} \exp\left[-x^2\left(\frac{1}{w_x^2}+\frac{ik}{2R_x}\right)-y^2\left(\frac{1}{w_y^2}+\frac{ik}{2R_y}\right)\right]. \quad (3.18)$$

The *ABCD* law holds for any paraxial optical system that can be described by a succession of thin lenses and free space elements. This covers a wide range of applications. Since the *ABCD* law holds for the passage of the Gaussian beam through any individual element of the system, and since the matrix of beam transmission through combination of these elements is obtained by multiplication of the individual matrices, the *ABCD* law holds for the entire optical system.

3.3 Field Distribution of Fiber

The field distribution in the core and cladding of a single-mode fiber is important in characterizing the fiber's optical performance. When solving Maxwell's equations for a step-index dielectric waveguide of circular cross-section, the single mode field propagated in the guide is made up of a Bessel function inside the core and a Hankel function in the cladding. Marcuse[53] has shown that the fields and power in a circularly symmetric step-index fiber are well approximated by Gaussian functions of radial position. In describing the propagation of an optical beam in step-index fibers, one defines the normalized frequency of the fiber as[53]

$$V = \frac{2\pi a}{\lambda}\sqrt{n_1^2 - n_2^2} = \frac{2\pi a}{\lambda} NA \ , \quad (3.19)$$

where n_1, n_2 are the refractive indices of the core and cladding, respectively, a

the radius of the core, and $NA = (n_1^2 - n_2^2)^{1/2}$ is the numerical aperture of the fiber. The number of propagating modes in the step-index fiber is proportional to its V number. The condition for the single-mode (the fundamental EH_{11} mode) operation is $V < 2.405$[53]. In terms of a quantity

$$\Delta = \frac{n_1 - n_2}{n_1} , \tag{3.20}$$

representing the relative refractive index difference between the core and cladding, Equation (3.19) is rewritten as

$$V = \frac{2\pi a}{\lambda} n_1 \sqrt{2\Delta - \Delta^2} , \tag{3.21}$$

where $n_2 = n_1(1-\Delta)$. For small Δ, $\Delta^2 \ll 2\Delta$ and the normalized frequency becomes

$$V \approx \frac{2\pi a}{\lambda} n_1 \sqrt{2\Delta} . \tag{3.22}$$

The field distribution in a step-index single-mode fiber can be approximated within 1% error by a Gaussian profile, if the normalized frequency is in the range, $1.9 \leq V \leq 2.4$[53]. Because this condition holds for typical single-mode fibers, the field leaving the fiber end can be approximated by a symmetric fundamental Gaussian beam with its waist located at the fiber endface. It can be shown that the spot size w_f of the Gaussian field in the fiber is only a function of V. This function can be approximated to within a fraction of 1 percent by the empirical formula[53]

$$\frac{w_f}{a} = 0.65 + \frac{1.619}{V^{3/2}} + \frac{2.879}{V^6} . \tag{3.23}$$

This equation holds, of course, only for a step-index fiber. Hence, the actual mode field in a step-index fiber is to be modeled as the Gaussian field distribution

$$\psi_f = \left(\frac{2}{\pi}\right)^{\frac{1}{2}} \frac{1}{w_f} \exp\left(-\frac{x^2+y^2}{{w_f}^2}\right), \tag{3.24}$$

where the spot size w_f is given in terms of a and V by Equation (3.23). The field distribution has been normalized for unit power and the fiber axis is taken along the z axis and is lined up with the laser beam.

3.4 Coupling Efficiency

The coupling efficiency, η, is given in terms of the overlap integral[54,55] of the field distributions of the incident laser beam (ψ_s) and the fiber mode (ψ_f) in the reference plane:

$$\eta = \frac{\left|\int_{-\infty}^{\infty} \psi_s \psi_f^* ds\right|^2}{\int_{-\infty}^{\infty} |\psi_s|^2 ds \int_{-\infty}^{\infty} |\psi_f|^2 ds}, \tag{3.25}$$

where the asterisk indicates the complex conjugate. If the field distributions ψ_s and ψ_f are normalized for unit power, Equation (3.25) reduces to

$$\eta = |c|^2 = \left|\int_{-\infty}^{\infty} \psi_s \psi_f^* ds\right|^2 . \tag{3.26}$$

Here c is the coupling coefficient defined as

$$c = \int_{-\infty}^{\infty} \psi_s \psi_f^* ds . \tag{3.27}$$

Clearly, η sensitively depends on the degree of matching between the spot sizes and distributions of the laser and fiber modes. By inserting Equations (3.18) and (3.24) into Equation (3.26), one can explicitly obtain the coupling efficiency η. In so doing, the elements of ray matrix have to be evaluated in terms of specific microlenses used. In the following chapter, two kinds of microlenses will be analyzed in detail.

4. COUPLING EFFICIENCY USING A MICROLENS

This chapter develops the Gaussian beam theory of coupling for the case of microlenses. The transformation properties of the microlenses are described by their *ABCD* matrixes. We will assume that no reflection and aperture diffraction effects are introduced by the microlenses so as to simplify the algebraic derivations and at the same time provide the physical insight. A discussions regarding the diffraction effects due to the finite apertures of the lenses are presented in Chapter 5. The microlenses studied here are conical and hemispherical lenses, but, the theory is generally applicable to other lenses.

4.1 Conical Microlens

Consider a field amplitude, emanating from the laser diode and coupled into a monomode fiber via a conical lens. The tip of the lens is located d distance away from the output facet of the diode. The conical shape of radius a and height h can be fabricated by chemically etching the fiber core (see Figure 4.1). Central to the analysis of coupling efficiency is the derivation of the *ABCD* matrix of this optical system. As shown in Figure 4.2, the normal to the planar interface between the air ($n = 1$) and the conical lens (of index of refraction n_1)

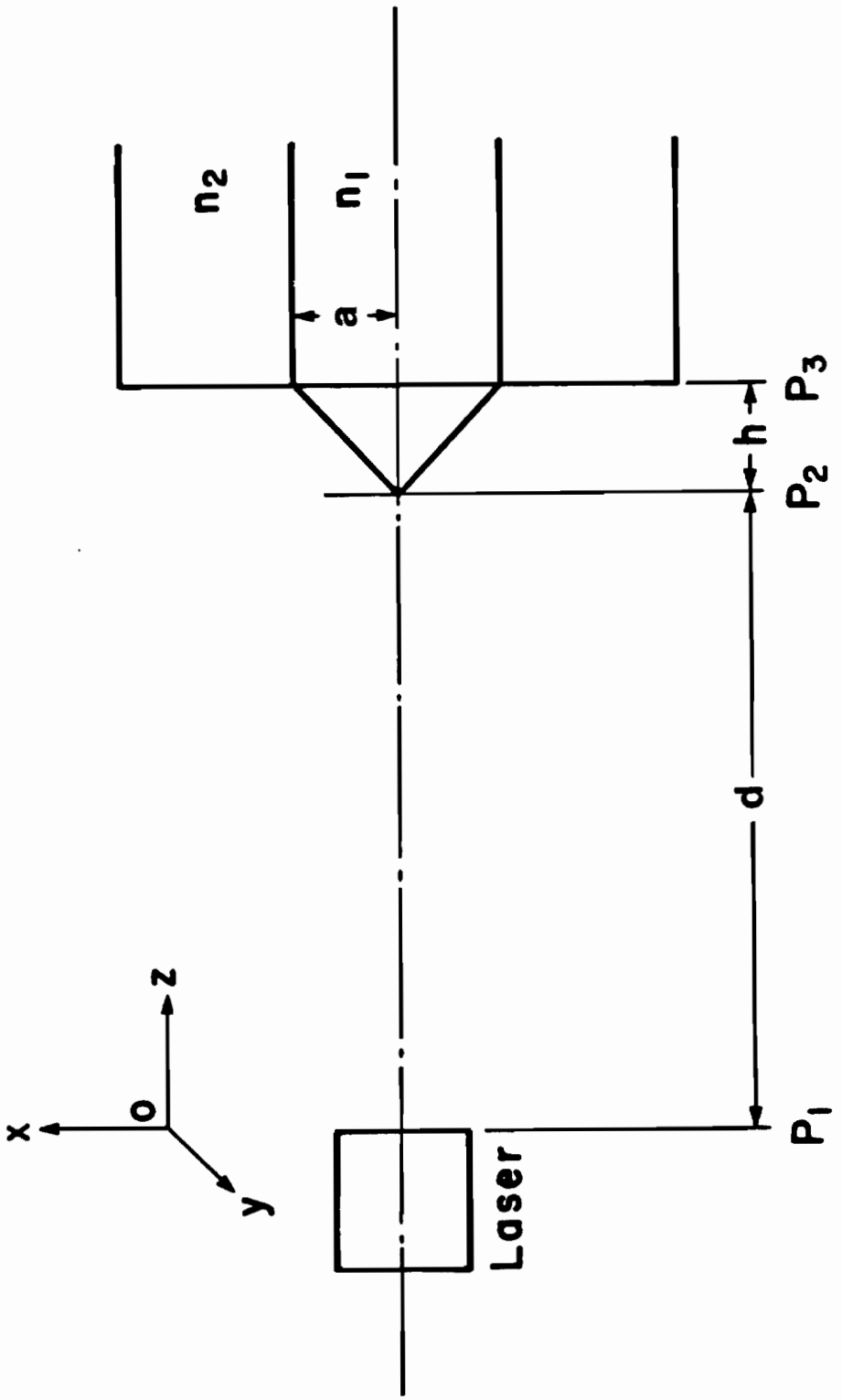

Figure 4.1 Schematic diagram for laser-to-fiber coupling via a conical microlens.

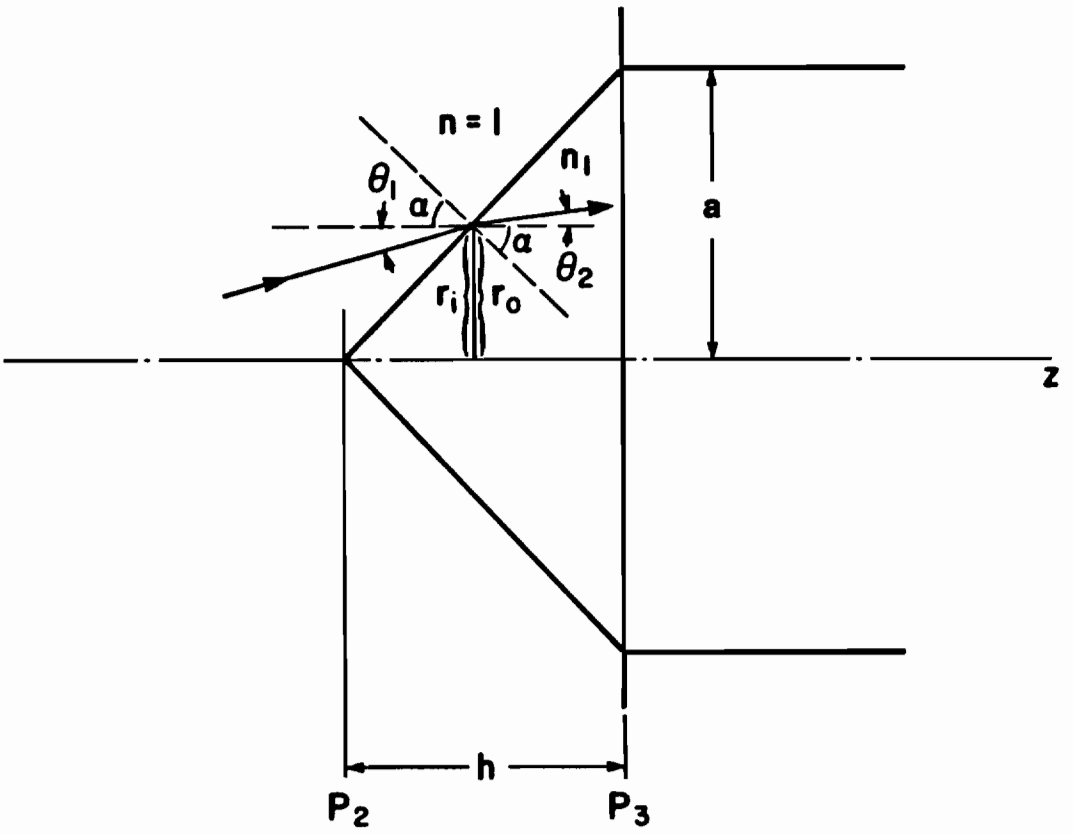

Figure 4.2 Schematic diagram for the refraction at the conical surface.

makes an angle α with the z-axis, taken here as the direction of propagation. A ray is incident at r_i at an angle θ_1 with respect to the z-axis, and propagates in the lens at angle θ_2 (Figure 4.2). From the Snell's law, one may write

$$\sin(\theta_1+\alpha) = n_1 \sin(\theta_2+\alpha) , \tag{4.1}$$

that is,

$$\sin\theta_1 \cos\alpha + \cos\theta_1 \sin\alpha = n_1(\sin\theta_2 \cos\alpha + \cos\theta_2 \sin\alpha) . \tag{4.2}$$

Under the conditions studied, it is a good approximation that $\sin\theta \approx \tan\theta \approx \theta$, and $\cos\theta \approx 1$ (see Figure 4.3). Equation (4.2) can be simplified as

$$\theta_1 \cos\alpha + \sin\alpha = n_1(\theta_2 \cos\alpha + \sin\alpha) . \tag{4.3}$$

One can express θ_2 in terms of θ_1, α and n_1 as

$$\theta_2 = \frac{\theta_1}{n_1} + \frac{1-n_1}{n_1} \tan\alpha , \tag{4.4}$$

where $\tan\alpha = h/a$. By introducing a notation,

$$\Delta\theta = (1-n_1)h/(n_1 a) , \tag{4.5}$$

one may write equation (4.4) as

$$\theta_2 = \frac{\theta_1}{n_1} + \Delta\theta . \tag{4.6}$$

The slope of input and output ray can be defined in the usual way, viz, $r_i' \approx \theta_1$ and $r_o' \approx \theta_2$. Hence, the relationship between r_o, r_o' and r_i, r_i' can be written in a matrix form as

$$\begin{bmatrix} r_o \\ r_o' \end{bmatrix} = \begin{bmatrix} 1 & 0 \\ 0 & 1/n_1 \end{bmatrix} \begin{bmatrix} r_i \\ r_i' \end{bmatrix} + \begin{bmatrix} 0 \\ \Delta\theta \end{bmatrix} . \tag{4.7}$$

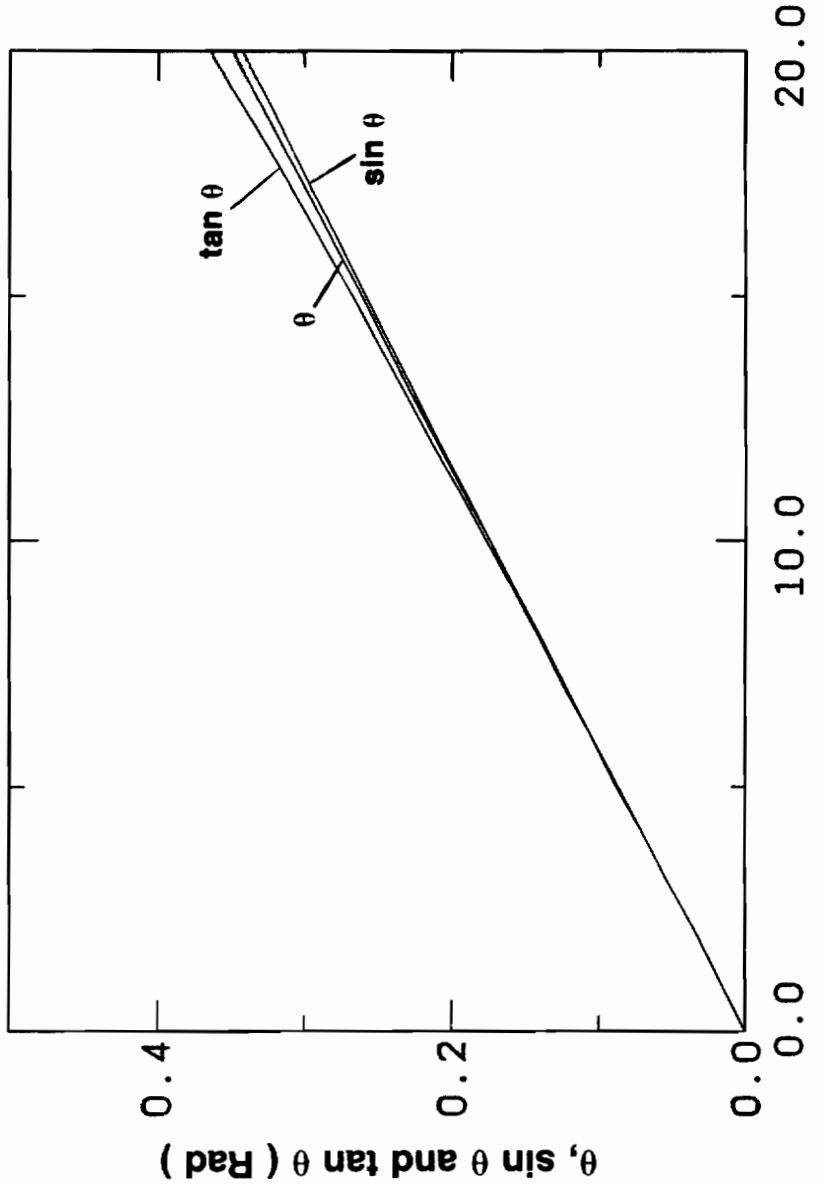

Figure 4.3 Values of sinθ, tanθ for small θ.

The 2×2-matrix in Equation (4.7) is identical to the *ABCD* matrix of the planar interface whose normal is parallel to the direction of propagation (see Figure 4.2). The second term in Equation (4.7) arises specifically due to the conical interface being slanted with respect to the z-axis, i.e., the normal to the interface making an angle α with respect to the z-axis. The role of the *ABCD* matrix appearing in Equation (4.7) is to transform the complex radius of curvature, q, as the beam traverses this interface. The second term incorporates the additional change in the slope of the output ray by an amount $\Delta\theta$ arising from α. The presence of this second term can therefore be accurately accounted for in the formulation by introducing the spatial mode function, $\exp(-ikr\Delta\theta)$, where $k=2n_1\pi/\lambda$ and $r=(x^2+y^2)^{1/2}$. With this mode function incorporating the additional refraction of the output beam, the optical system of the conical lens can be formally analyzed in terms of: (i) the propagation of the beam through the air by distance $d_l(r_i)$, (ii) refraction at the dielectric interface, whose normal is now parallel to the z-axis and (iii) the traversal of the beam through the lens of thickness $h_l(r_i)$. As a first order approximation, we will assume $h_l(r_i)=h$, and $d_l(r_i)=d$. Hence, the corresponding ray matrix reads as

$$\begin{bmatrix} A & B \\ C & D \end{bmatrix} = \begin{bmatrix} 1 & h \\ 0 & 1 \end{bmatrix} \begin{bmatrix} 1 & 0 \\ 0 & 1/n_1 \end{bmatrix} \begin{bmatrix} 1 & d \\ 0 & 1 \end{bmatrix} = \begin{bmatrix} 1 & d+h/n_1 \\ 0 & 1/n_1 \end{bmatrix} . \tag{4.8}$$

The field distribution of the laser diode at the P_3-plane (Figure 4.1) is thus given by

$$\psi_s = \left(\frac{2}{\pi}\frac{1}{w_x w_y}\right)^{\frac{1}{2}} \exp\left[-x^2\left(\frac{1}{w_x^2}+\frac{ik}{2R_x}\right)-y^2\left(\frac{1}{w_y^2}+\frac{ik}{2R_y}\right)\right.$$

$$-ik\Delta\theta\sqrt{x^2+y^2}\Big]\,, \tag{4.9}$$

where w_x, w_y, R_x and R_y are to be evaluated explicitly in terms of given system parameters from Equations (3.16), (3.17) and (4.8). Upon inserting Equations (3.24) and (4.9) into Equation (3.26), one can find the coupling efficiency for this conical lens system.

4.1.1 Conical Microlens for Circular Laser Beam

When the symmetry with respect to x and y holds, the expressions of the laser field distribution (Equation (4.9)) and the fiber field distribution (Equation (3.24)) reduce to simple forms as

$$\psi_s = \left(\frac{2}{\pi}\right)^{\frac{1}{2}} \frac{1}{w} \exp\left[-r^2\left(\frac{1}{w^2}+\frac{ik}{2R}\right)-ik\Delta\theta\, r\right], \tag{4.10}$$

$$\psi_f = \left(\frac{2}{\pi}\right)^{\frac{1}{2}} \frac{1}{w_f} \exp\left(-\frac{r^2}{w_f^2}\right). \tag{4.11}$$

Substitution of above equations into Equation (3.27) leads to

$$c = \frac{4}{ww_f}\int_0^\infty \exp\left[-r^2\left(\frac{1}{w_f^2}+\frac{1}{w^2}+\frac{ik}{2R}\right)-ik\Delta\theta r\right] r dr\,. \tag{4.12}$$

Taking

$$\alpha_r = \frac{1}{w_f^2}+\frac{1}{w^2}\,, \tag{4.13}$$

$$\beta_r = \frac{k}{2R} , \tag{4.14}$$

$$\gamma = k\Delta\theta , \tag{4.15}$$

Equation (4.12) can be rewritten as

$$c = \frac{4}{ww_f}\int_0^\infty e^{-\alpha_r r^2 - i(\beta_r r^2+\gamma r)} r dr$$

$$= \frac{4}{ww_f}\int_0^\infty e^{-\alpha_r r^2}[\cos(\beta_r r^2+\gamma r) - i\sin(\beta_r r_2+\gamma r)] r dr$$

$$= \frac{4}{ww_f}(X_c - iY_c) , \tag{4.16}$$

where

$$X_c = \int_0^\infty e^{-\alpha_r r^2}\cos(\beta_r r^2+\gamma r) r dr , \tag{4.17}$$

$$Y_c = \int_0^\infty e^{-\alpha_r r^2}\sin(\beta_r r^2+\gamma r) r dr . \tag{4.18}$$

We obtain the coupling efficiency as

$$\eta = |c|^2 = \left(\frac{4}{ww_f}\right)^2 (X_c^2 + Y_c^2) . \tag{4.19}$$

Figure 4.4 presents the coupling efficiency, η, vs the distance (d/a) between the laser and the lens. Here the laser beam spot size was taken to be symmetrical, i.e., $w_x = w_y$. The different η-curves correspond to different heights, h, of the lens. For a given conical lens, i.e., fixed h/a, there exists an optimal distance, d/a

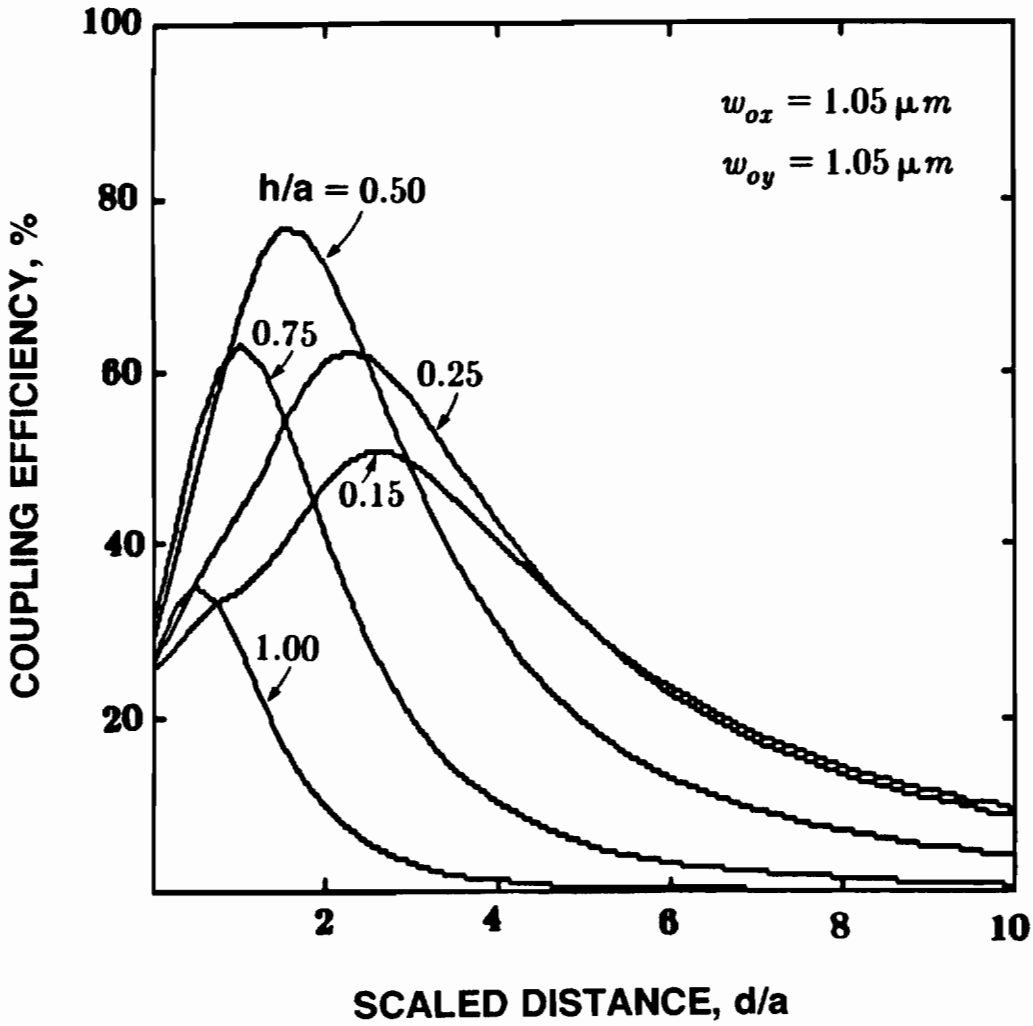

Figure 4.4 Coupling efficiency vs laser-to-fiber distance for different heights of the etched cone. The beam spot size was taken to be symmetric.

at which η attains the maximum value. This trend is general and can be explained based on the radius of curvature (R_x, R_y) and spot size (w_x, w_y) of the beam that are imaged onto the P_3-plane (Figure 4.1). For this purpose, typical values of R_x and w_x of the symmetrical laser beam are plotted as a function of d/a in Figure 4.5. When the tip of the conical lens closes the laser facet plane, i.e., $d/a=0$, spot size w_x of the laser beam is minimum at the fiber end. It is smaller than the spot size of the fiber mode and the divergence of the laser beam is large as it enters in the fiber, consequently the coupling efficiency is low (Figure 4.4). With increasing d/a, w_x increases monotonically, while R_x decreases sharply due to a strong refraction of the beam at the interface of the conical lens. The effect of the former is to reduce the beam divergence, whereas decreasing R_x enhances the divergence. Inasmuch as η strongly depends on the degree of beam divergence, in the region where $0<d/a<0.5$, η is determined by these two opposing tendencies. On the other hand, when the fiber is moved far away from the laser, the spot size w_x becomes larger than the radius of the fiber core, and only part of the laser beam can be intercepted by the fiber. Obviously, the coupling efficiency is also low, and gets lower as the fiber is further away. It therefore becomes clear that there should exist an optimal distance, d/a, at which these two opposite tendencies give rise to the maximum possible η value.

The maximum efficiency, η_{max}, discussed in the preceding paragraph depends, in turn, on the shape of the lens, namely the height, h/a. Specifically, for $a=4\mu m$, η_{max} can be high as 80% at $h/a=0.5$. Any departure of h from this value on both sides results in considerably smaller η_{max} as shown in Figure 4.4. This can be qualitatively understood as follows. Ideally, the role of the lens

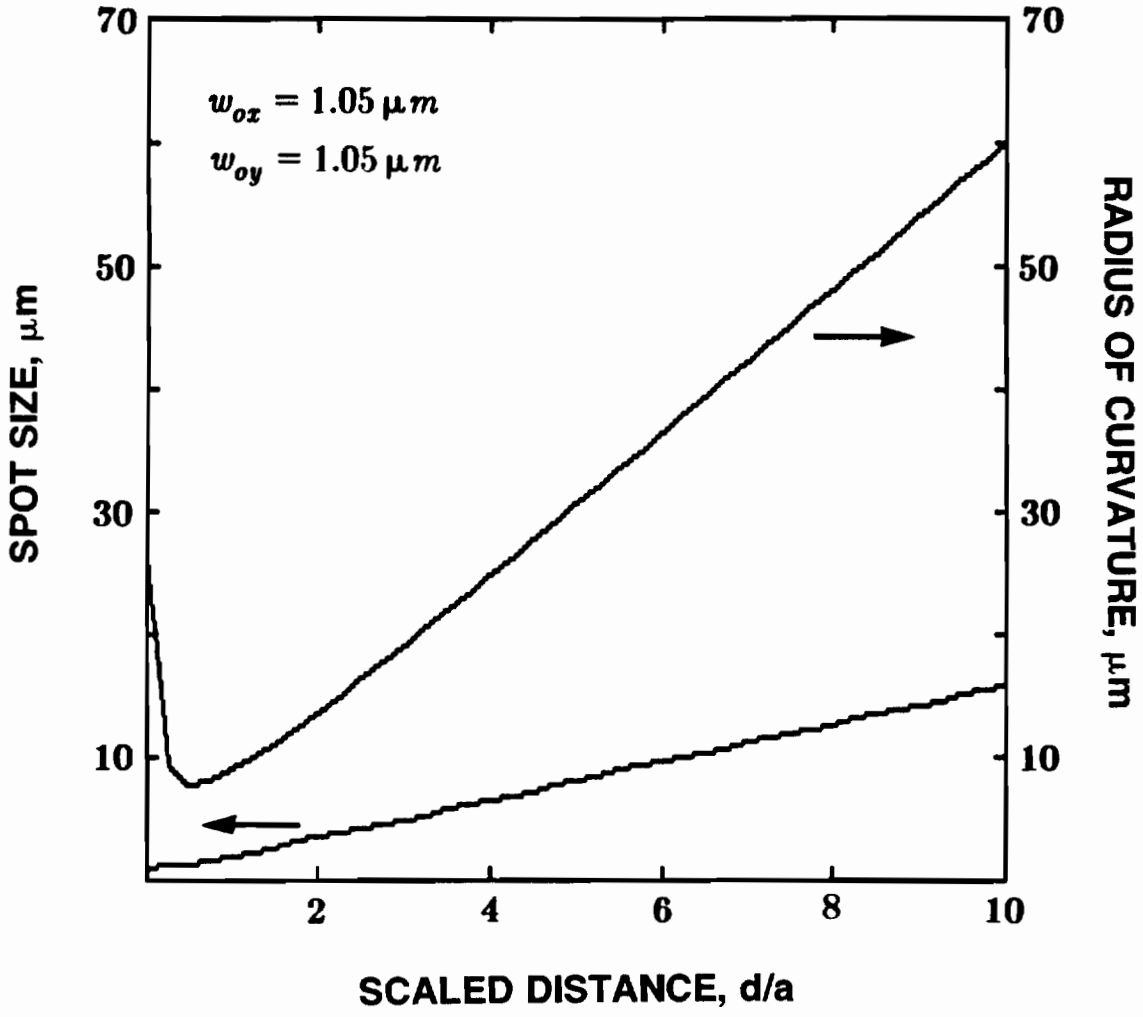

Figure 4.5 Beam spot size and radius of curvature at the base of conical fiber vs laser-to-fiber distance.

consists of guiding a given laser field amplitude in such a way that on the P_3-plane the field distribution is matched exactly with the fiber mode function (see Equation (3.24)). In practice, however, there is always considerable mismatch in the spot size and the radius of curvature. The optimal matching of these quantities should depend strongly on the shape of the lens, h/a, as well as the distance, d/a.

4.1.2 Conical Microlens for Elliptic Laser Beam

Consider the effect of an asymmetrical laser beam spot size on η. Upon inserting Equations (3.24) and (4.9) into Equation (3.27), one can get the coupling coefficiency

$$c = \frac{2}{\pi w_f}\left(\frac{1}{\omega_x w_y}\right)^{\frac{1}{2}} \int_{-\infty}^{\infty}\int_{-\infty}^{\infty} \exp\left[-\left(\frac{1}{w_f^2}+\frac{1}{w_x^2}+\frac{ik}{2R_x}\right)x^2\right.$$

$$\left.-\left(\frac{1}{w_f^2}+\frac{1}{w_y^2}+\frac{ik}{2R_y}\right)y^2 - ik\Delta\theta\sqrt{x^2+y^2}\right] dxdy \ . \tag{4.20}$$

Taking

$$\alpha_x = \frac{1}{w_f^2} + \frac{1}{w_x^2} \ , \tag{4.21}$$

$$\alpha_y = \frac{1}{w_f^2} + \frac{1}{w_y^2} \ , \tag{4.22}$$

$$\beta_x = \frac{k}{2R_x} \ , \tag{4.23}$$

$$\beta_y = \frac{k}{2R_y} , \tag{4.24}$$

Equation (4.20) becomes

$$c = \frac{2}{\pi w_f}\left(\frac{1}{w_x w_y}\right)^{\frac{1}{2}} \int_{-\infty}^{\infty}\int_{-\infty}^{\infty} e^{-(\alpha_x x^2+\alpha_y y^2)-i\left(\beta_x x^2+\beta_y y^2+\gamma\sqrt{x^2+y^2}\right)} dxdy$$

$$= \frac{2}{\pi w_f}\left(\frac{1}{w_x w_y}\right)^{\frac{1}{2}} \int_{-\infty}^{\infty}\int_{-\infty}^{\infty} e^{-(\alpha_x x^2+\alpha_y y^2)}\left[\cos\left(\beta_x x^2+\beta_y y^2+\gamma\sqrt{x^2+y^2}\right)\right.$$

$$\left. -i\sin\left(\beta_x x^2+\beta_y y^2+\gamma\sqrt{x^2+y^2}\right)\right] dxdy$$

$$= \frac{2}{\pi w_f}\left(\frac{1}{w_x w_y}\right)^{\frac{1}{2}} (X_a - iY_a) , \tag{4.25}$$

where

$$X_a = \int_{-\infty}^{\infty}\int_{-\infty}^{\infty} e^{-(\alpha_x x^2+\alpha_y y^2)}\cos\left(\beta_x x^2+\beta_y y^2+\gamma\sqrt{x^2+y^2}\right) dxdy , \tag{4.26}$$

$$Y_a = \int_{-\infty}^{\infty}\int_{-\infty}^{\infty} e^{-(\alpha_x x^2+\alpha_y y^2)}\sin\left(\beta_x x^2+\beta_y y^2+\gamma\sqrt{x^2+y^2}\right) dxdy . \tag{4.27}$$

The coupling efficiency is given by

$$\eta = |c|^2 = \frac{4}{\pi^2 w_f^2 w_x w_y}(X_a^2 + Y_a^2). \tag{4.28}$$

In Figure 4.6 η is presented as a function of d/a for fixed h/a and w_{ox} but for different w_{oy}. As can be clearly observed, the value of $\eta_{\max}$ decreases significantly with increasing degree of ellipticity, i.e., $w_{oy} - w_{ox}$. This is to be

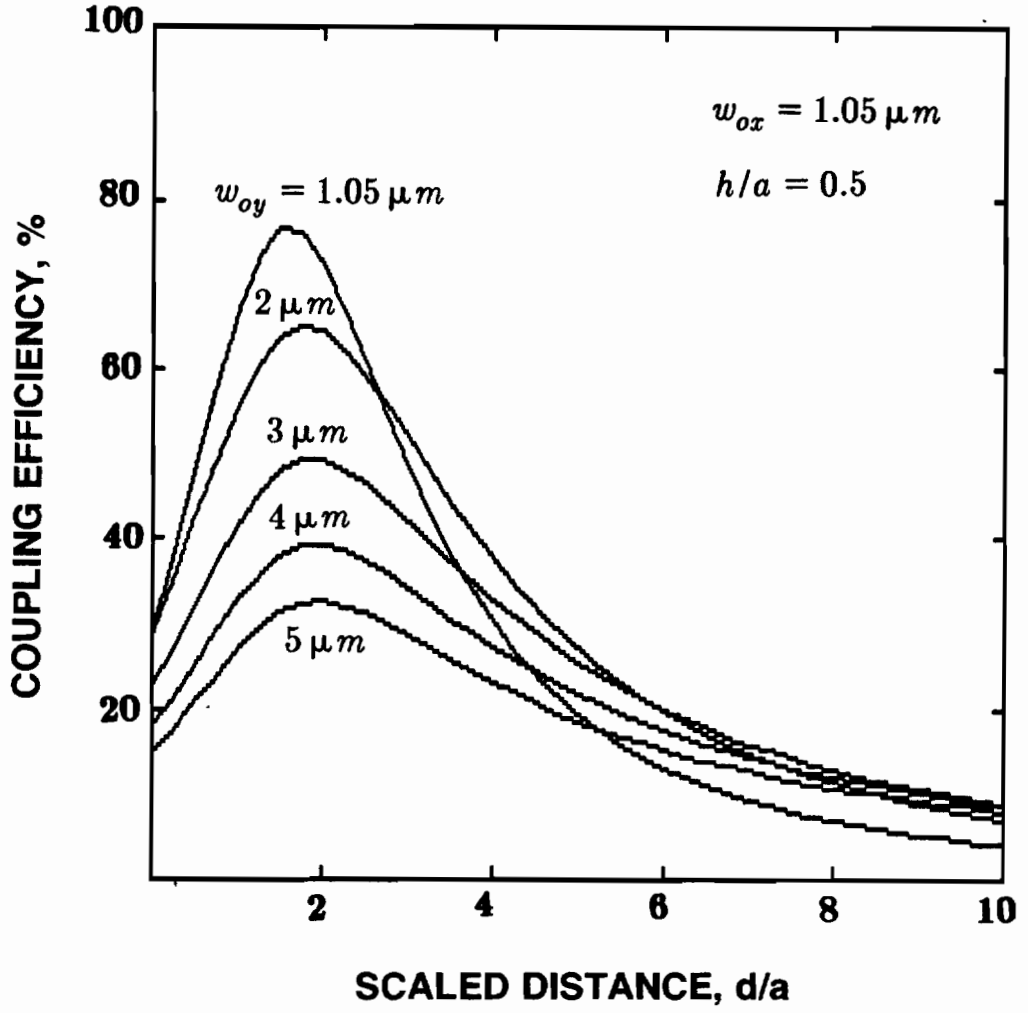

Figure 4.6 Coupling efficiency of conical lens vs laser-to-fiber distance for different ellipticity of the laser beam.

anticipated, since the conical lens is azimuthally symmetric and the fiber mode function is also circularly symmetric. However, for a fixed value of $w_{oy} - w_{oz}$, the value of η_{max} can be considerably enhanced by optimizing the height of the lens. This is specifically illustrated in Figure 4.7.

4.2 Hemispherical Microlens

The conical lens could be fire-polished or melted into a hemispherical lens of the same volume. The hemispherical lens is believed to be more efficient in guiding the laser beam into the fiber than the conical lens[17]. In this section, its coupling efficiency is analyzed in detail and compared with that of conical lens. The transformation matrix of this optical system again consists of three components: (i) free space propagation of ray by distance d, (ii) refraction at the hemispherical interface and (iii) the traversal of the ray through the lens of thickness h_s. Hence, one may write

$$\begin{bmatrix} A & B \\ C & D \end{bmatrix} = \begin{bmatrix} 1 & h_s \\ 0 & 1 \end{bmatrix} \begin{bmatrix} 1 & 0 \\ (1-n_1)/n_1 r_l & 1/n_1 \end{bmatrix} \begin{bmatrix} 1 & d \\ 0 & 1 \end{bmatrix}, \tag{4.29}$$

where the quantity, $h_s = r_l - (r_l^2 - a^2)^{1/2}$ is given in terms of the radius of curvature of the lens, r_l, and a. The laser field distribution at the P_3-plane then reads as

$$\psi_s = \left(\frac{2}{\pi} \frac{1}{w_x w_y} \right)^{\frac{1}{2}} \exp\left[-x^2 \left(\frac{1}{w_x^2} + \frac{ik}{2R_x} \right) - y^2 \left(\frac{1}{w_y^2} + \frac{ik}{2R_y} \right) \right], \tag{4.30}$$

where w_x, w_y, R_x and R_y are to be evaluated explicitly in terms of given parameters from Equations (3.16), (3.17) and (4.29).

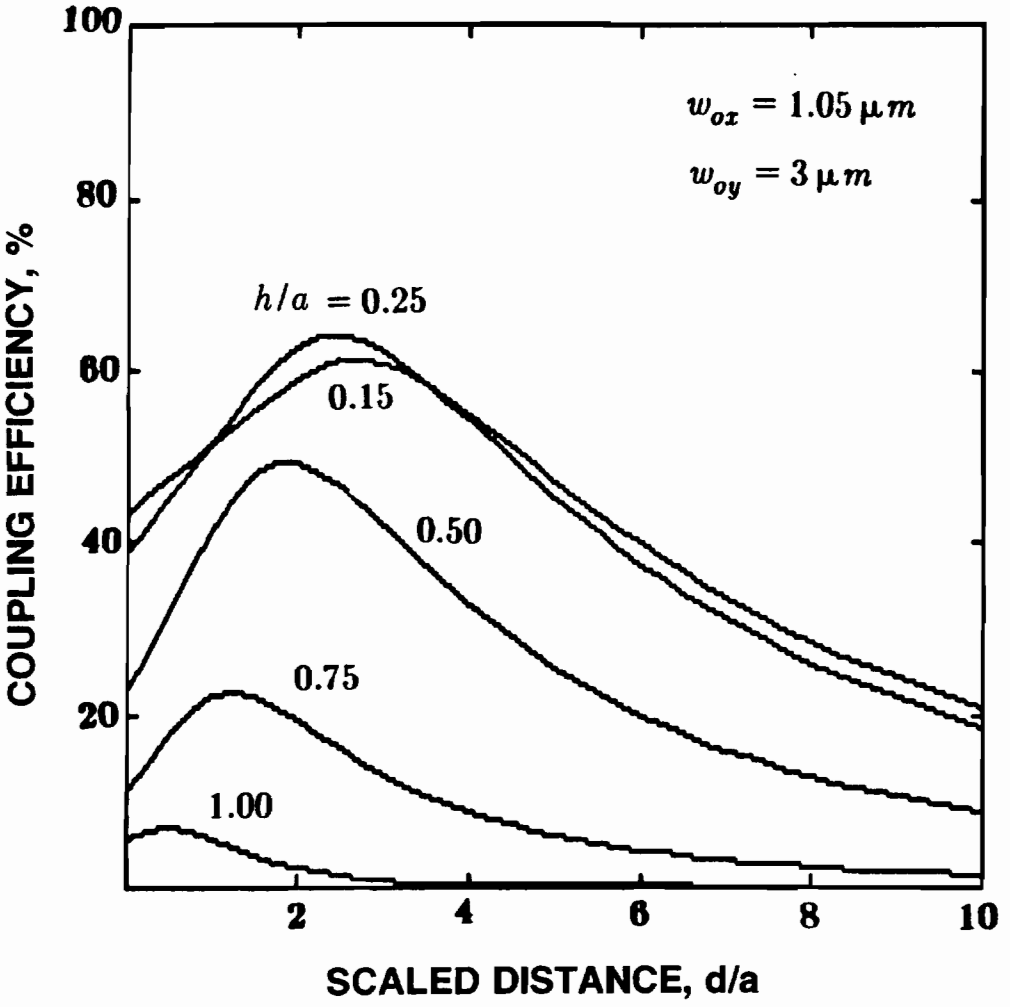

Figure 4.7 Coupling efficiency vs laser-to-fiber distance for an elliptic beam spot size and different heights of the etched cone.

4.2.1 Hemispherical Microlens for Circular Laser Beam

For a circular laser beam, the expression of the laser field distribution is

$$\psi_s = \left(\frac{2}{\pi}\right)^{\frac{1}{2}} \frac{1}{w} e\left[-r^2\left(\frac{1}{w^2}+\frac{ik}{2R}\right)\right]. \tag{4.31}$$

Upon inserting Equations (4.31) and (4.11) into Equation (3.27) we get

$$c = \frac{4}{w_f w}\int_0^\infty e^{-q'r^2} r dr, \tag{4.32}$$

where we have defined the parameter q' as

$$q' = \frac{1}{w_f^2}+\frac{1}{w^2}+\frac{ik}{2R}. \tag{4.33}$$

The result of Equation (4.32) is expressed as

$$c = \frac{2}{w_f w q'}. \tag{4.34}$$

Substitution of Equations (4.33) and (4.34) into Equation (3.26) then yield

$$\eta = \frac{4}{\left(\frac{w}{w_f}+\frac{w_f}{w}\right)^2+\left(\frac{k}{2R}w_f w\right)^2}. \tag{4.35}$$

Figure 4.8 presents the coupling efficiency, η as a function of distance (d/a) for three different radii, r_l of hemispherical lens. Here, the laser beam was taken to be symmetrical. For fixed r_l, there exists an optimal distance at which η attains the maximum value. This again can be understood in terms of the spot size and the radius of curvature of the laser beam that are imaged onto the P_3-

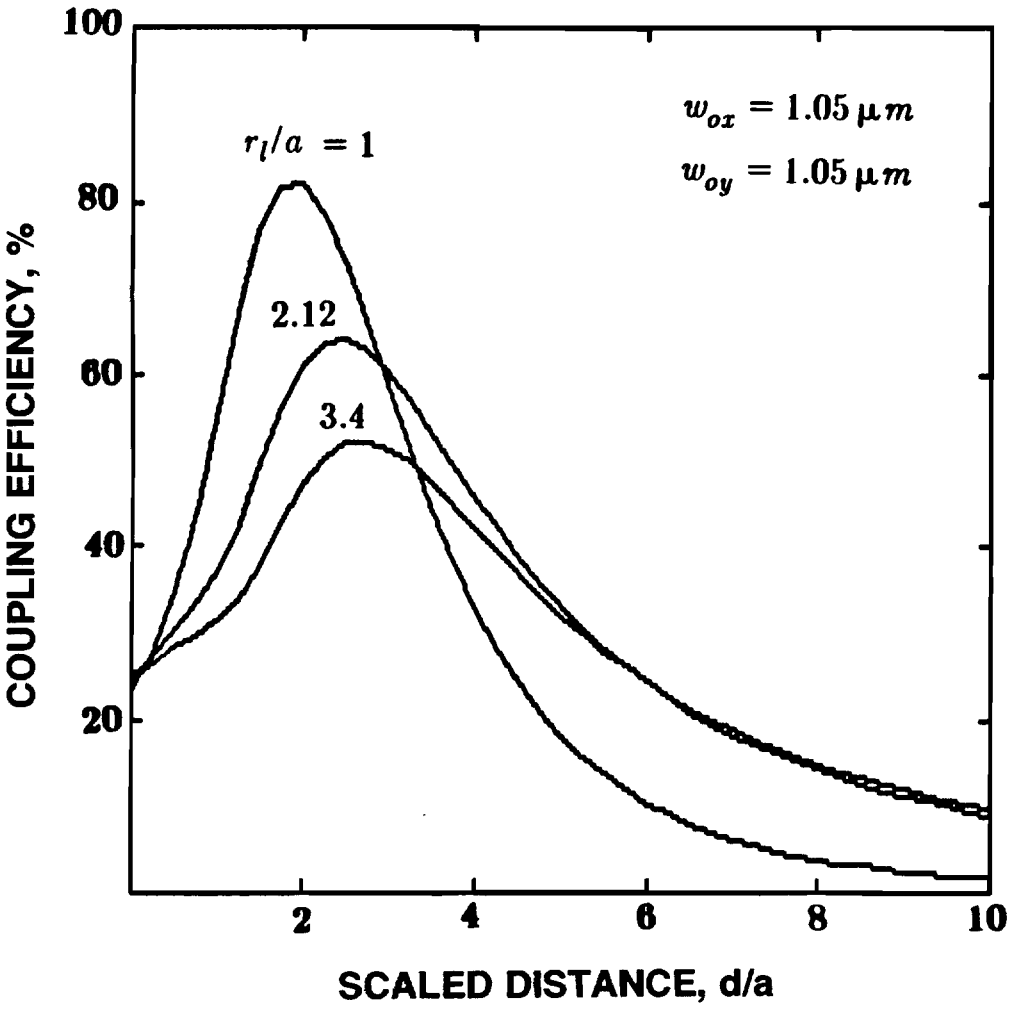

Figure 4.8 Coupling efficiency vs laser-to-fiber distance for different radius of curvature of the hemispheric lens. The beam spot size was taken to be symmetric.

plane (see Figures 4.4 and 4.5). A coupling efficiency as high as 82% may be attained using optimally designed hemispherical lens. This value is slightly larger than the corresponding value of 75% for the case of conical lens.

4.2.2 Hemispherical Microlens for Elliptical Laser Beam

For an elliptical laser beam, substitution of Equations (4.30) and (3.24) into Equation (3.27) leads to

$$c = \frac{2}{\pi}\frac{1}{w_f}\left(\frac{1}{w_x w_y}\right)^{\frac{1}{2}} \int_{-\infty}^{\infty}\int_{-\infty}^{\infty} e^{-q_x' x^2} e^{-q_y' y^2} dx dy \ , \tag{4.36}$$

where

$$q_x' = \frac{1}{w_f^2} + \frac{1}{w_x^2} + \frac{ik}{2R_x} \ , \tag{4.37}$$

$$q_y' = \frac{1}{w_f^2} + \frac{1}{w_y^2} + \frac{ik}{2R_y} \ , \tag{4.38}$$

Equation (4.36) can be rewritten as

$$c = \frac{2}{\pi}\frac{1}{w_f}\left(\frac{1}{w_x w_y}\right)^{\frac{1}{2}} 4\int_0^{\infty} e^{-q_x' x^2} dx \int_0^{\infty} e^{-q_y' y^2} dy$$

$$= \frac{2}{\pi}\frac{1}{w_f}\left(\frac{1}{w_x w_y}\right)^{\frac{1}{2}} \left(\frac{\pi}{q_x'}\right)^{\frac{1}{2}} \left(\frac{\pi}{q_y'}\right)^{\frac{1}{2}}$$

$$= \frac{2}{w_f}\left(\frac{1}{w_x w_y q_x' q_y'}\right)^{\frac{1}{2}} . \tag{4.39}$$

Substitution of Equations (4.37), (4.38) and (4.39) into Equation (3.26) then yields

$$\eta = \frac{\dfrac{4}{w_f^2 w_x w_y}}{\left[\left(\dfrac{1}{w_f^2}+\dfrac{1}{w_x^2}\right)^2+\left(\dfrac{k}{2R_x}\right)^2\right]^{\frac{1}{2}}\left[\left(\dfrac{1}{w_f^2}+\dfrac{1}{w_y^2}\right)^2+\left(\dfrac{k}{2R_y}\right)^2\right]^{\frac{1}{2}}} . \quad (4.40)$$

In Figure 4.9, η vs d/a curves are presented for various nonsymmetrical laser beam spot sizes. With the increasing degree of nonsymmetry, i.e. $w_{oy} - w_{ox}$, η is reduced significantly, as expected. Again, for given w_{ox} and w_{oy}, the η-value can be considerably enhanced with the optimal design of hemispherical lens, as illustrated in Figure 4.10.

We should point out that the application of the *ABCD* law will only give exact results for paraxial rays. Up to this point, we ignored the continuous lateral expansion of the laser beam on its way towards the coupling microlens. If the source spot size is sufficiently small, the emitted beam will exhibit a considerable divergence. In that case, the intensity of the incoming beam is expanded over the whole of the optical system entrance aperture stop formed by the microlens rim, so the diffraction effect becomes noticeable[58] and the field will be different from that obtained using the *ABCD* law. An analysis investigating the diffraction field distribution is developed in the next chapter.

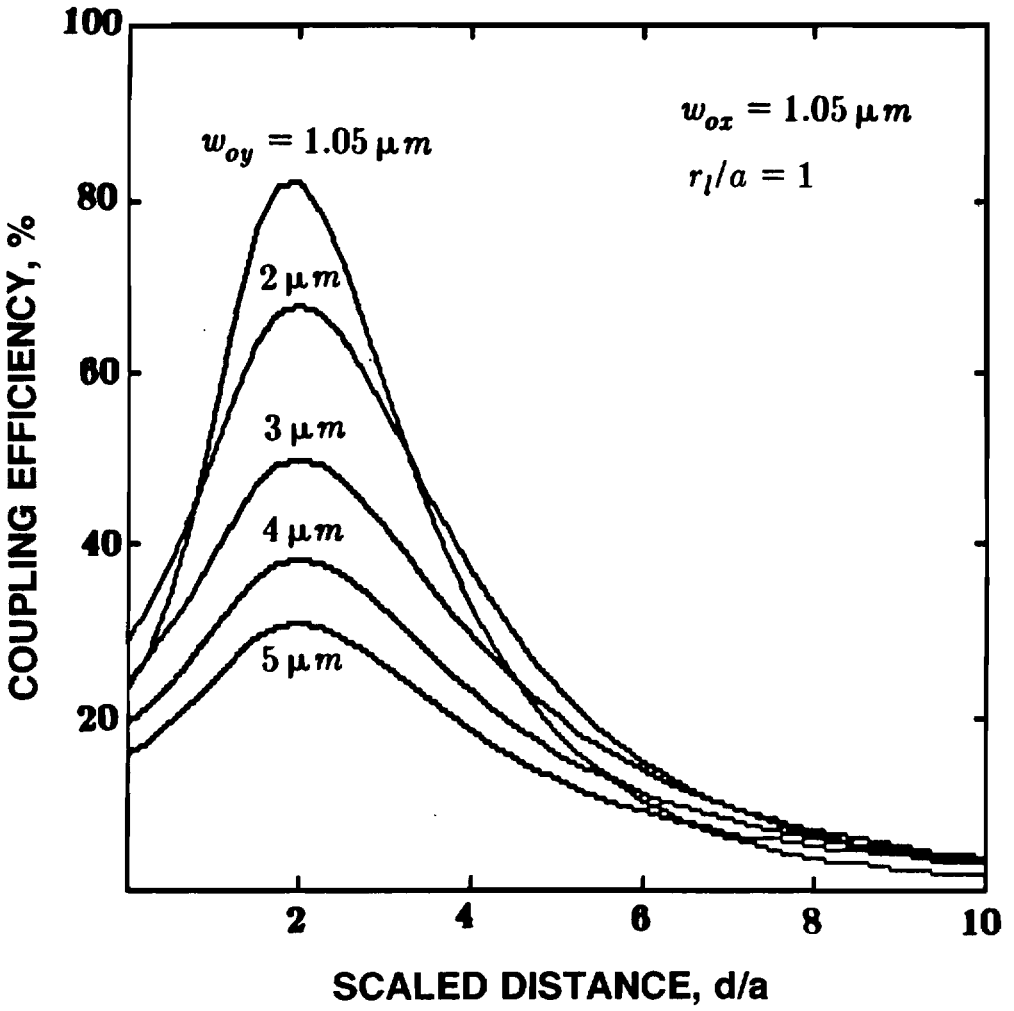

Figure 4.9 Coupling efficiency of hemispheric lens vs laser-to-fiber distance for different beam spot sizes.

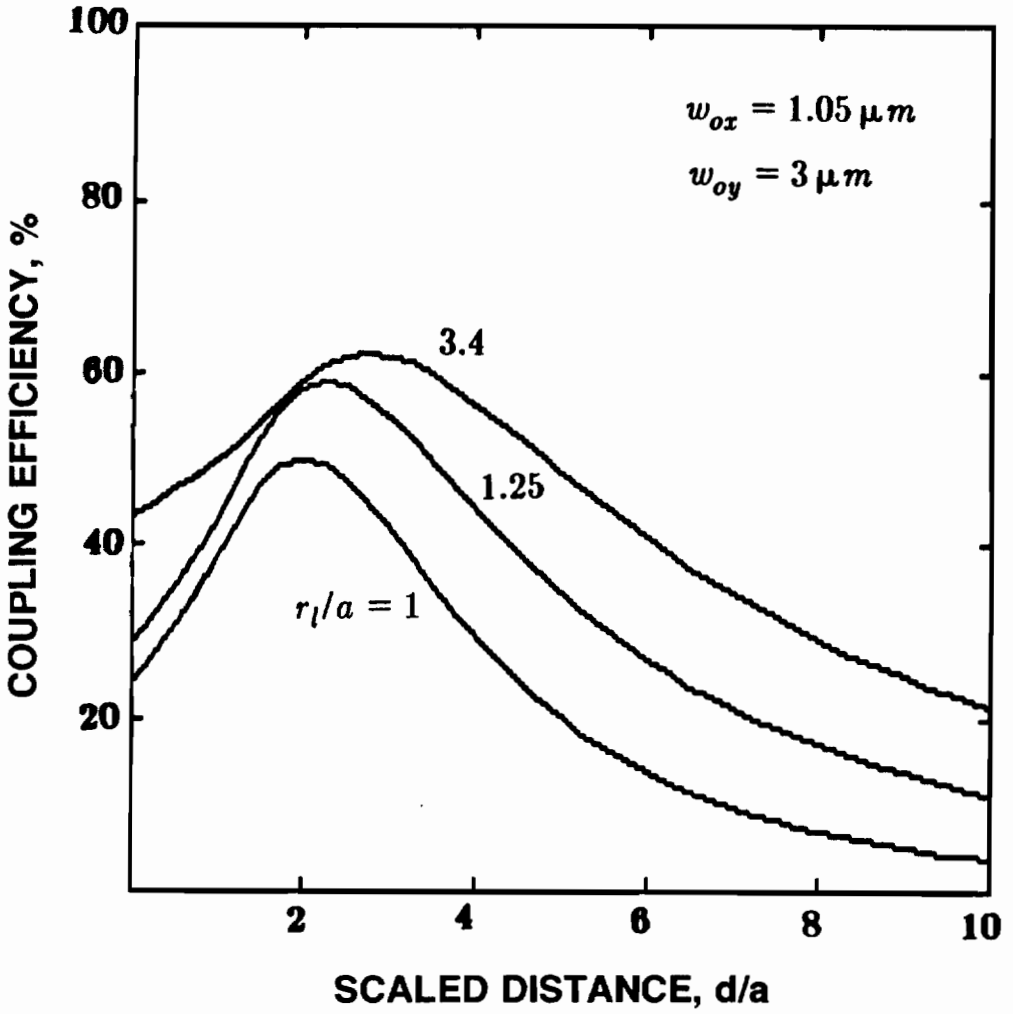

Figure 4.10 Coupling efficiency vs laser-to-fiber distance for an elliptic beam spot size and different radius of curvature of hemispheric lens.

5. DIFFRACTION EFFECT OF THE MICROLENS

The transformation of the laser beam by lenses is described by the *ABCD* law in Chapter 3. It allows one to trace the Gaussian beam through any optical structures for which the elements of the transformation matrix can be obtained. However, the *ABCD* law is a good approximation only when the lens aperture is much larger than the beam spot size[57]. When the aperture of the microlens is of the same order as the beamwidth, the diffraction phenomenon becomes noticeable[56, 58]. For microlenses, the diffraction theory should, perhaps, be used to calculate the diffracted field after the microlens. From a rigorous mathematical point of view, of course, the theory of diffraction is one of the most complicated topics in classical physics[59]. This is partly because boundary conditions are very complicated for real physical diffraction surfaces, which will partially absorb, partially reflect, and partially scatter the incident light. It involves solving the wave equation in the presence of an awkward boundary, and only under very special circumstances can an exact solution be obtained[60]. Such a solution usually presents great mathematical difficulties. Here, this author uses some physical ideas along with principles of the classical electrodynamics to study this problem while neglecting absorption, reflection and scattering. Investigating the diffraction effect on the microlens will boil down to solving the Dirichlet

boundary-value problem of the Helmholtz wave equation with a Green function. The analysis based on the generalized Helmholtz-Kirchhoff's diffraction formula is derived in this chapter. The results are compared with those using the *ABCD* law.

5.1 The Field on the Microlens Surface

To find the field in the microlens, it is required to know or approximate the value of the field, Ψ, on the microlens surface first. It may be performed by means of the vector form of the field and the electromagnetic boundary conditions at interface between different media. In the following discussion, the Gaussian units will be used throughout.

Consider that the electromagnetic fields of a Gaussian beam in vacuum can be described by a complex vector potential $\mathbf{A}$[61], and suppose that $\mathbf{A}$ is polarized along y axis:

$$\mathbf{A} = \frac{c}{\omega} u e^{-ikz} \hat{y} , \tag{5.1}$$

where c is the velocity of light in vacuum, ω is the frequency and u is a Gaussian description defined by

$$u = \left(\frac{2}{\pi}\right)^{\frac{1}{2}} \frac{1}{w} \exp\left[-(x^2+y^2)\left(\frac{1}{w^2}+\frac{ik}{2R}\right)\right] . \tag{5.2}$$

The divergence of $\mathbf{A}$ is

$$\nabla\cdot\mathbf{A} = \frac{\partial}{\partial y}\left(\frac{c}{\omega} u e^{-ikz}\right) = \frac{c}{\omega} e^{-ikz} \frac{\partial u}{\partial y} . \tag{5.3}$$

According to the Lorentz condition[62]

$$\nabla\cdot\mathbf{A} + \frac{1}{c}\frac{\partial\Phi}{\partial t} = 0\,, \tag{5.4}$$

the scalar potential Φ is expressed in terms of the divergence of $\mathbf{A}$

$$\Phi = -i\frac{c}{\omega}\nabla\cdot\mathbf{A}\ . \tag{5.5}$$

The gradient of Φ is derived as

$$\begin{aligned}
\nabla\Phi &= -i\frac{c}{\omega}\nabla(\nabla\cdot\mathbf{A}) \\
&= -i\frac{c^2}{\omega^2}\nabla\left(e^{-ikz}\frac{\partial u}{\partial y}\right) \\
&= -i\frac{c^2}{\omega^2}e^{-ikz}\left[\frac{\partial^2 u}{\partial x\partial y}\hat{x} + \frac{\partial^2 u}{\partial y^2}\hat{y} + \left(\frac{\partial^2 u}{\partial y\partial z} - ik\frac{\partial u}{\partial y}\right)\hat{z}\right] \\
&= -\frac{c}{\omega}e^{-ikz}\frac{\partial u}{\partial y}\hat{z}\ ,
\end{aligned} \tag{5.6}$$

where $k=\omega/c$ has been used, and $|\partial^2 u/\partial x\partial y|$, $|\partial^2 u/\partial y^2|$ and $|\partial^2 u/\partial y\partial z|$ have been ignored compared with $k|\partial u/\partial y|$, because u is assumed to have a slow dependence compared to the rapid variation of the exponential factor[61,63,46,52,64].

Thus, obtain the electric field vector[62]

$$\mathbf{E} = -\frac{1}{c}\frac{\partial\mathbf{A}}{\partial t} - \nabla\Phi = iue^{-ikz}\hat{y} + \frac{c}{\omega}e^{-ikz}\frac{\partial u}{\partial y}\hat{z}\ . \tag{5.7}$$

It is clear now that u denotes the transverse component of the electric field[61,63,46,52]. The longitudinal component of the electric field is very small and

has only a contribution to the near field. For this reason, the following derivations only involve the transverse component of the electric field of the incident light from the laser diode,

$$\mathbf{E}^i = E_y^i \hat{y} = ue^{-ikz}\hat{y} \ . \tag{5.8}$$

When this field falls on the surface of the hemispherical microlens, the field $\mathbf{E}$ across the surface is governed by the electric boundary conditions. For a hemispherical surface, the inward normal of the surface is described as

$$\mathbf{n} = -\frac{x}{r_l}\hat{x} - \frac{y}{r_l}\hat{y} + \frac{1}{r_l}\sqrt{r_l^2-(x^2+y^2)}\hat{z} \qquad \text{for } x^2+y^2 \le r_l^2 \ . \tag{5.9}$$

The tangential components of $\mathbf{E}$ on either side of the boundary are related by[62]

$$(\mathbf{E}_2-\mathbf{E}_1)\times\mathbf{n} = 0 \ , \tag{5.10}$$

$$\text{i.e.,} \qquad \begin{vmatrix} \hat{x} & \hat{y} & \hat{z} \\ n_x & n_y & n_z \\ E_x & E_y & E_z \end{vmatrix} = \begin{vmatrix} \hat{x} & \hat{y} & \hat{z} \\ n_x & n_y & n_z \\ 0 & E_y^i & 0 \end{vmatrix}, \tag{5.11}$$

where E_x, E_y and E_z are components of the field inside the surface, and n_x, n_y and n_z are components of the surface normal $\mathbf{n}$ defined in Equation (5.9). And the normal components of $\mathbf{D}$ on either side of the boundary are related by[62]

$$(\mathbf{D}_2-\mathbf{D}_1)\cdot\mathbf{n} = 0 \ , \tag{5.12}$$

$$\text{i.e.,} \qquad n_xE_x + n_yE_y + n_zE_z = \frac{1}{n_1^2}n_yE_y^i \ , \tag{5.13}$$

where $\mathbf{D}=\epsilon\mathbf{E}$ has been used and $n_1=(\mu\epsilon)^{1/2}$ is the index of refraction of the microlens, ϵ is the permittivity and the magnetic permeability $\mu\approx 1$. From Equa-

tion (5.11) and (5.13), one gets a set of algebra equations

$$n_x E_x + n_y E_y + n_z E_z = \frac{1}{n_1^2} n_y E_y^i \,, \tag{5.14}$$

$$n_z E_x - n_x E_z = 0 \,, \tag{5.15}$$

$$n_y E_x - n_x E_y = -n_x E_y^i \,. \tag{5.16}$$

We can solve this set of equations for E_x, E_y and E_z, obtaining

$$E_x = \left(\frac{1}{n_1^2} - 1\right) n_x n_y E_y^i \,, \tag{5.17}$$

$$E_y = \left(\frac{1}{n_1^2} - 1\right) n_y^2 E_y^i + E_y^i \,, \tag{5.18}$$

$$E_z = \left(\frac{1}{n_1^2} - 1\right) n_y n_z E_y^i \,. \tag{5.19}$$

The amplitude of this field $\mathbf{E}$ across the surface of the microlens yields

$$|\mathbf{E}| = \sqrt{E_x^2 + E_y^2 + E_z^2} = g(\mathbf{x}) E_y^i \,, \tag{5.20}$$

where

$$g(\mathbf{x}) = \left[\left(\frac{1}{n_1^4} - 1\right) n_y^2 + 1\right]^{\frac{1}{2}} \,. \tag{5.21}$$

Now the value of $\Psi(\mathbf{x})$ on the boundary surface S can be specified in terms of the amplitude of the field $\mathbf{E}$,

$$\Psi(\mathbf{x}) = g(\mathbf{x}) u e^{-ikz} \,. \tag{5.22}$$

5.2 Generalized Kirchhoff Integral

Consider a strictly monochromatic scalar field $\psi(\mathbf{x})$, and let it have harmonic time dependence, $e^{-i\omega t}$. The field $\psi(\mathbf{x})$ is assumed to satisfy the scalar Helmholtz wave equation inside V that is a volume bounded by a closed surface S. Here $\psi(\mathbf{x})$ also denotes the field that we want in the microlens. We are then led to the Dirichlet boundary-value problem with the nonhomogeneous boundary condition

$$(\nabla^2 + k^2)\,\psi(\mathbf{x}) = 0 \qquad \text{in } V\,, \tag{5.23}$$

$$\psi(\mathbf{x}) = \Psi \qquad \text{on } S\,, \tag{5.24}$$

where Ψ is defined by Equation (5.22) in previous section. This problem will be solved by means of a Green function.

First of all, let us try to introduce a Green function for the Helmholtz wave equation $G(\mathbf{x},\mathbf{x}')$, defined by

$$(\nabla^2 + k^2)\,G(\mathbf{x},\mathbf{x}') = -\delta(\mathbf{x},\mathbf{x}')\,. \tag{5.25}$$

The Green function $G(\mathbf{x},\mathbf{x}')$ is independent of Ψ; that is, it depends on the differential equation and the position of two points: the observation point, where the field is measured, represented by $\mathbf{x}$, and the source point, where the unit source is placed, represented by $\mathbf{x}'$. One has by Green's theorem[62]

$$\iiint_V (\phi\nabla^2\psi - \psi\nabla^2\phi)\,dV = -\iint_S \left[\phi\frac{\partial\psi}{\partial n'} - \psi\frac{\partial\phi}{\partial n'}\right] dS\,, \tag{5.26}$$

where $\partial/\partial n'$ denotes differentiation along the inward normal to S. We put $\phi = G$, $\psi = \psi$, make use of the wave equations (5.23) and (5.25) in Green's

theorem, and obtain[62]

$$\psi(\mathbf{x}) = \iint_S \left[\psi(\mathbf{x}') \frac{\partial G(\mathbf{x},\mathbf{x}')}{\partial n'} - G(\mathbf{x},\mathbf{x}') \frac{\partial \psi(\mathbf{x}')}{\partial n'} \right] dS \ . \tag{5.27}$$

This equation holds if $\mathbf{x}$ is inside V; if it is not, the left-hand side vanishes. Equation (5.27) is a rigorous mathematical expression following from the wave equation. By taking G to be the infinite space Green function describing outgoing waves,

$$G(\mathbf{x},\mathbf{x}') = \frac{e^{ikR}}{4\pi R} \ , \tag{5.28}$$

where $\mathbf{R} = \mathbf{x} - \mathbf{x}'$, the Kirchhoff integral formula reads[65]

$$\psi(\mathbf{x}) = \frac{1}{4\pi} \iint_s \left[\psi(\mathbf{x}') \frac{\partial}{\partial n'} \left(\frac{e^{ikR}}{R} \right) - \frac{e^{ikR}}{R} \frac{\partial \psi(\mathbf{x}')}{\partial n'} \right] dS \ , \tag{5.29}$$

with the integration only over the surface S of the diffracting screen.

In order to apply Equation (5.29), it is necessary to know the values of ψ and $\partial\psi/\partial n'$ on the surface S. Unless the problem has been solved by other means, these values are not known. Kirchhoff's approach was to approximate the values of ψ and $\partial\psi/\partial n'$ on S, that is, (i) ψ and $\partial\psi/\partial n'$ vanish everywhere on S except in the openings; (ii) the values of ψ and $\partial\psi/\partial n'$ in the openings are equal to the values of the incident wave in the absence of any screen. The standard diffraction calculations of classical optics are all based on this Kirchhoff approximation. It is obvious that the recipe can have only limited validity. There is, in fact, a serious mathematical inconsistency in the assumptions of Kirchhoff[62]. It can be shown for the Helmhotz wave equation (5.23), as well as for the Laplace equation, that if ψ and $\partial\psi/\partial n'$ are both zero on any finite surface, then $\psi=0$

everywhere. Thus the only mathematically correct consequence of the first Kirchhoff assumption is that the diffracted field vanishes everywhere. This is, of course, inconsistent with the second assumption. Furthermore, Equation (5.29) does not yield on S the assumed values of ψ and $\partial\psi/\partial n'$. It must be emphasized, therefore, that ψ and its normal derivative are not both arbitrary on S. As a boundary condition we might have ψ specified on S or $\partial\psi/\partial n'$ specified on S, or even a combination of ψ and $\partial\psi/\partial n'$ specified on S, but not both separately.

The mathematical inconsistencies in the Kirchhoff approximation can be removed by the choice of a proper Green function[62] in Equation (5.27). The Green function can be constructed which is appropriate to Dirichlet boundary condition[62]

$$G_D(\mathbf{x},\mathbf{x}') = 0 \qquad \text{for } \mathbf{x}' \text{ on } S \ . \tag{5.30}$$

Then the second term in the surface integral in Equation (5.27) vanishes and Equation (5.27) is reduced to

$$\psi(\mathbf{x}) = \iint_S \Psi(\mathbf{x}') \frac{\partial G_D(\mathbf{x},\mathbf{x}')}{\partial n'} dS \ . \tag{5.31}$$

This is the solution of the nonhomogeneous boundary-value problem and is also a generalized Kirchhoff integral. It expresses a scalar field $\psi(\mathbf{x})$ inside the volume bounded by the closed surface S in terms of the value of the field Ψ on the boundary surface S. Hence, we not only avoid the mathematical inconsistencies in the Kirchhoff approximation but also effect significant mathematical simplifications in the given problem.

5.3 Determination of Dirichlet Green Function

It should be clear, that the boundary conditions have the drastic effect on the form of the Green function. It is rather involved to determine the Green function because of its dependence on the shape of the surface S. In order to simplify the discussion, let us consider the circumstance of a hemispherical microlens in which the surface S is a small hemispherical drum of radius r_l upon a sheet, as shown in Figure 5.1. Since the problem is in three dimensions, it is not surprising that the determination of the Green function associated with the problem would present very serious practical difficulties. Fortunately, the method of images[66] can be used so that it is a relatively straightforward matter to obtain the following Dirichlet Green function satisfied the Dirichlet boundary condition in Equation (5.30):

$$G_D(\mathbf{x},\mathbf{x}_1') = \frac{1}{4\pi}\left(\frac{e^{ikR_1}}{R_1} - \frac{r_l}{r_0}\frac{e^{ikR_2 r_0/r_l}}{R_2} - \frac{e^{ikR_3}}{R_3} + \frac{r_l}{r_0}\frac{e^{ikR_4 r_0/r_l}}{R_4}\right) \quad (5.32)$$

where $r_0=|\mathbf{x}_1'|$, $R_1=|\mathbf{x}-\mathbf{x}_1'|$, $R_2=|\mathbf{x}-\mathbf{x}_2'|$, $R_3=|\mathbf{x}-\mathbf{x}_3'|$, and $R_4=|\mathbf{x}-\mathbf{x}_4'|$, $\mathbf{x}_2'$, $\mathbf{x}_3'$ and $\mathbf{x}_4'$ being three images of $\mathbf{x}_1'$. Explicitly one has[67]

$$\frac{\partial G_D(\mathbf{x},\mathbf{x}_1')}{\partial n'} = \nabla G_D(\mathbf{x},\mathbf{x}_1')\cdot\mathbf{n}\ , \quad (5.33)$$

where $\mathbf{n}$ is inward normal of the hemispherical surface described by Equation (5.9). Using Equations (5.32) and (5.9) in Equation (5.33), we obtain, after some laborious algebra, the following expression of the normal derivative of $G_D(\mathbf{x},\mathbf{x}_1')$ on the surface S:

$$\frac{\partial G_D(\mathbf{x},\mathbf{x}_1')}{\partial n'} = \frac{1}{2\pi}\frac{r_l^2-r_0^2}{r_l}\frac{e^{ikR_1}}{R_1^2}\left(\frac{1}{R_1}-ik\right). \quad (5.35)$$

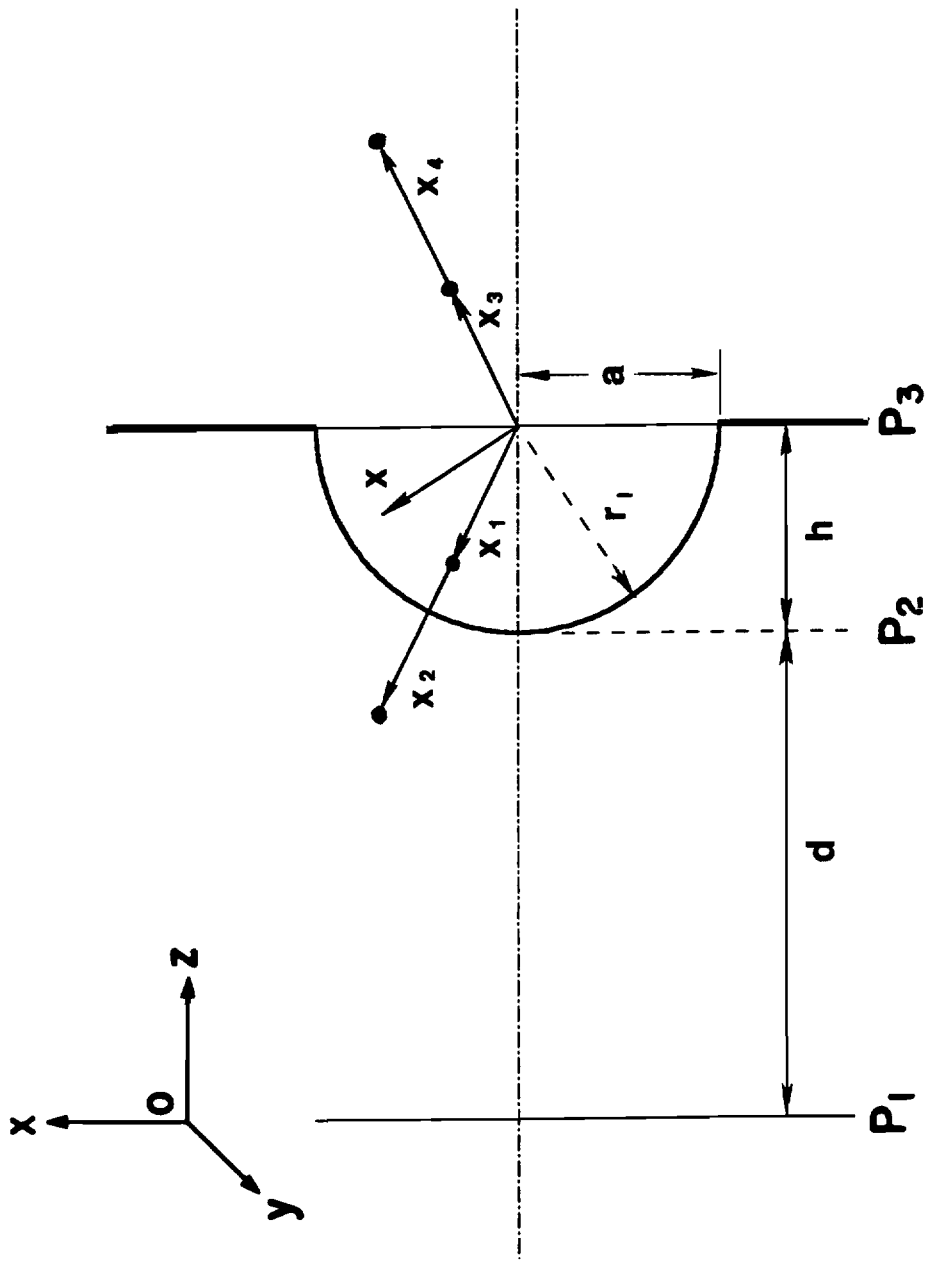

Figure 5.1 Schematic diagram for the solution of Dirichlet Green function by method of images.

Then the generalized Kirchhoff integral (5.31) becomes

$$\psi(\mathbf{x}) = \frac{r_l^2 - r_0^2}{4\pi r_l} \int\int_S \Psi(\mathbf{x}') \frac{e^{ikR_1}}{R_1^2} \left(\frac{1}{R_1} - ik \right) dS \ , \tag{5.36}$$

where the surface integral goes over the curved hemispherical surface, $\psi(\mathbf{x})$ expresses the field inside the microlens. The integral presentation in Equation (5.36) is similar to the Poisson's integral formula. Since the field Ψ on surface S of the microlens has been specified by Equation (5.22), the problem is formally solved.

5.4 Evaluation of the Field on the Microlens Basis

The surface integral in Equation (5.36) can be reduced to a double integral. The hemispherical surface has the equation

$$z = d + r_l - \sqrt{r_l^2 + (x^2 + y^2)} \ , \tag{5.37}$$

where d is the distance between the laser output facet and the tip of the microlens. Thus

$$\frac{\partial z}{\partial x} = \frac{x}{\sqrt{r_l^2 - (x^2 + y^2)}} \ , \tag{5.38}$$

$$\frac{\partial z}{\partial y} = \frac{y}{\sqrt{r_l^2 - (x^2 + y^2)}} \ , \tag{5.39}$$

and

$$\begin{aligned} dS &= \sqrt{1 + (\partial z/\partial x)^2 + (\partial z/\partial y)^2} \ dxdy \\ &= \frac{r_l}{\sqrt{r_l^2 - (x^2 + y^2)}} \ dxdy \ . \end{aligned} \tag{5.40}$$

In cylindrical coordinates, dS can be written as

$$dS = \frac{r_l}{\sqrt{r_l^2 - r'^2}} r' dr' d\phi' . \tag{5.41}$$

The explicit form of Equation (5.36) is therefore

$$\psi(r,\phi) = \frac{r_l^2 - r^2}{4\pi} \int_0^{2\pi} \int_0^a \frac{\Psi(r',\phi')}{\sqrt{r_l^2 - r'^2}} \frac{e^{ikR_1}}{R_1^2} \left(\frac{1}{R_1} - in_1 k \right) r' dr' d\phi' , \tag{5.42}$$

where a is the radius of the microlens circular aperture. Substitution of Equation (5.22) for Ψ in Equation (5.42) leads to

$$\psi(r,\phi) = \frac{r_l^2 - r^2}{(2\pi)^{3/2}} \int_0^{2\pi} \int_0^a \frac{r' g(r',\phi') e^{-(r'/w)^2}}{w R_1^2 \sqrt{r_l^2 - r'^2}} \left(\frac{1}{R_1} - in_1 k \right)$$

$$\times \exp\left[-ikn_1 \left(\frac{r'^2}{2R_1} + d + r_l - \sqrt{r_l^2 - r'^2} - R_1 \right) \right] dr' d\phi' , \tag{5.43}$$

where

$$R_1 = \sqrt{r^2 + r_l^2 - 2r' r (\cos\phi' \cos\phi + \sin\phi' \sin\phi)} , \tag{5.44}$$

$$g(r',\phi') = \left[\left(\frac{1}{n_1^4} - 1 \right) \left(\frac{r' \sin\phi'}{r_l} \right)^2 + 1 \right]^{\frac{1}{2}} . \tag{5.45}$$

Equation (5.43) expresses the laser field distribution at the P_3-plane (Figure 5.1). Upon inserting Equation (3.24) and (5.45) into Equation (3.25), one can obtain the coupling efficiency for the microlens coupling system.

5.5 Results of the Coupling Efficiency

To demonstrate the above formalism, the calculations have been performed for a $r_l = 4.35\mu m$ microlens with an index of refraction of 1.4509 for different distance of the microlens tip from the laser.

The numerical integration in Equation (5.43) is evaluated by the method, described by Patterson, of the optimum addition of points to Gauss quadrature formulae[68].

Figure 5.2 shows that the coupling efficiencies calculated by diffraction theory compare with those calculated by *ABCD* law. When we included the diffraction effect, the coupling efficiency is predicted to give 32.6% instead of 37.7% (*ABCD* law) for $d = 5\mu m$, 55.3% instead of 63% for $d = 8\mu m$ and 35.4% instead of 46.9% for $d = 12\mu m$. The discrepancy is 5.1% for $d = 5\mu m$, 7.7% for $d = 8\mu m$ and 11.5% for $d = 12\mu m$.

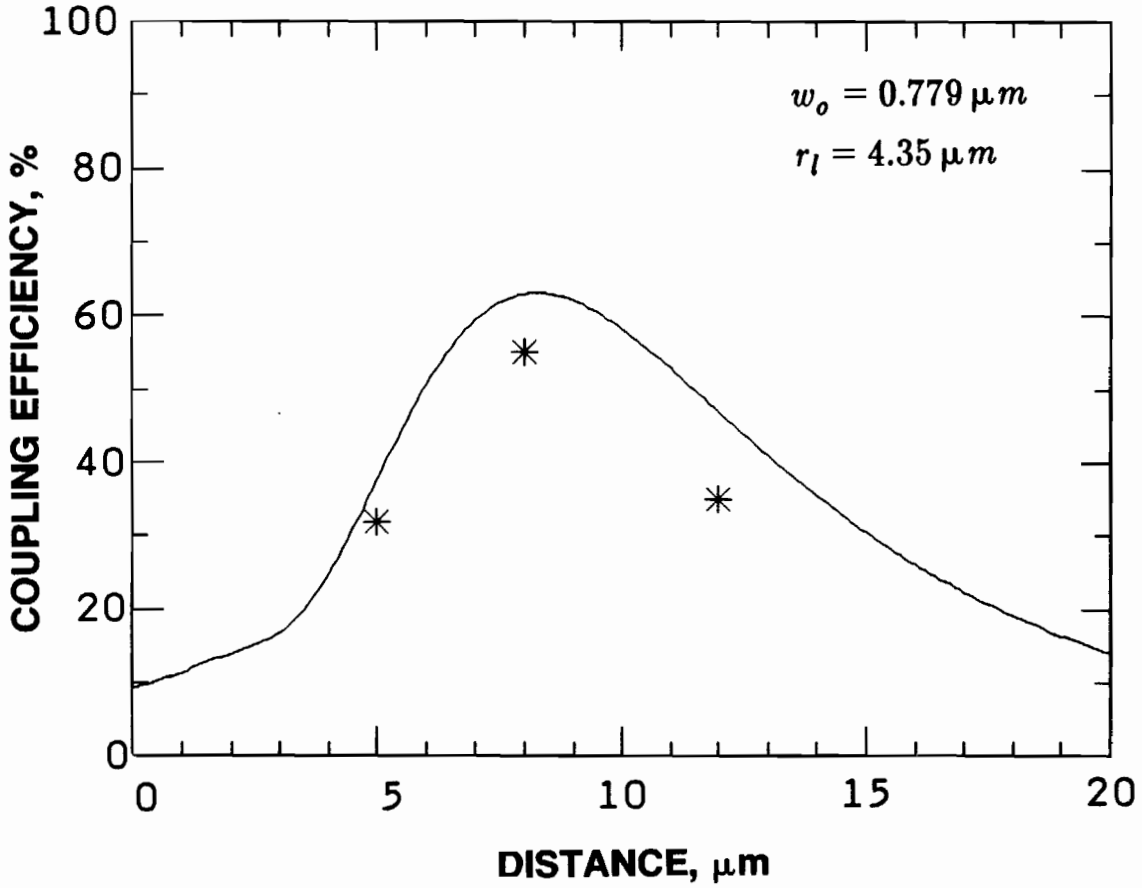

Figure 5.2 Coupling effiencies calculated by diffraction theory (star *) compare with those calculated by ABCD law (solid line -).

6. FABRICATION AND EXPERIMENT

The fabrication of microlenses and experimental results for coupling efficiency of a buried heterostructure InGaAsP semiconductor laser to a single-mode fiber using a etched microlens are discussed in this chapter. The results of coupling loss characteristics, both with and without a microlens, are compared with the theoretically calculated values.

6.1 Fabrication of Microlenses

Microlenses with diameter and height of the order of a few microns cannot be fabricated by means of conventional polishing or melting techniques. It is also very difficult to mount and align these microlenses in an optical system. Several methods have been proposed to solve the fabrication and alignment problems:

(a) controlled exposure with guided light, development and curing of a photoresist deposited onto the fiber end[69],

(b) microsphere coupling lens positioned with high-accuracy micropositioners and glued onto the fiber end[37,38],

(c) self-centering of a microsphere coupling lens using adhesive surface tension and gravity[70],

(d) tapered hemispherical end, obtained by drawing the fiber in an arc discharge, and[40]

(e) chemically etching out a lens-like structure in the core region at the fiber end[41,17].

Using different process techniques, excellent results have been reported with coupling efficiency between laser diode and single-mode fiber well in excess of -3 dB. The etching method, however, seems to be most convenient and relatively simple to implement, since this method is a true self-centering process. It requires no additional material deposition, and is amenable to batch processing.

The etching method is based on a well-known process, which is routinely used to reveal the refractive-index profile of an optical fiber: when a silica fiber end is dipped into a hydrofluoric acid solution, there is a differential etching speed between the core and the cladding. The single-mode fibers are fabricated by the vapor-phase axial deposition (VAD) method. The fiber is composed of a 3 mol% GeO_2 doped SiO_2 core with pure SiO_2 cladding. The relative refractive index difference is 0.3%, the refractive index of the core 1.4509, the core diameter 8.7 μm, the cutoff wavelength 1.2 μm, the normalized frequency 2.3, and calculated spot size $w_f = 4.93$ μm. The fiber parameters used are summarized in Table 6.1. The etchant solution consists of one part 50% hydrofluoric (HF) acid buffered in 10 parts of 40% ammonium fluoride (NH_4F). The etching rate is highest in the pure silica cladding region and lowest in the central portion of the core where the Ge concentration is highest. This differential etch process results in a conical feature in the central light-carrying area of the fiber.

Table 6.1. Parameters of Single-Mode Fiber Used in Coupling Experiment

Core diameter ϕ_{co}	8.7μm
Cladding diameter ϕ_{cl}	125μm
Coating diameter ϕ_{ca}	250μm
Maximum attenuation (at 1.3 μm)	0.5%
Maximum total dispersion (at 1.3 μm)	3.5ps/nm km
Relative refractive index difference Δ	0.3%
Cutoff wavelength λ_c	1.27μm
Normalized frequency V (at 1.3 μm)	2.3
Numerical aperture N.A.	0.11
Mode spot size w_f	4.93μm

The sequential change in the fiber end structure with increasing etching time is shown schematically in Figure 6.1. The height of the etched-out mesa at the core region increases with increasing etching time and finally a finite circular cone is formed. Figure 6.2 shows a micrograph of a conical microlens taken by a scanning electron microscope (SEM). The bases of the fabricated conical lenses are equal to the core cross section. The base angle θ of the circular cone in Figure 6.1 can be related to the etching rates of the core and cladding regions with the following simple equation[71]:

$$V_{core} \cos\theta = V_{clad} , \tag{6.1}$$

where V_{core} is the etching rate of the core and V_{clad} is the etching rate of the cladding. By adjusting the temperature of the solution, the concentration of HF, and the process time, the height of the cone can be controlled over a wide range. Using this etching process, microlenses are relatively easy to fabricate, reproducible, and automatically aligned with the the fiber core.

Successive fire polishing after the etching process converts easily etched-out mesa or cone structure into a round-shaped microlens structure[71]. Several

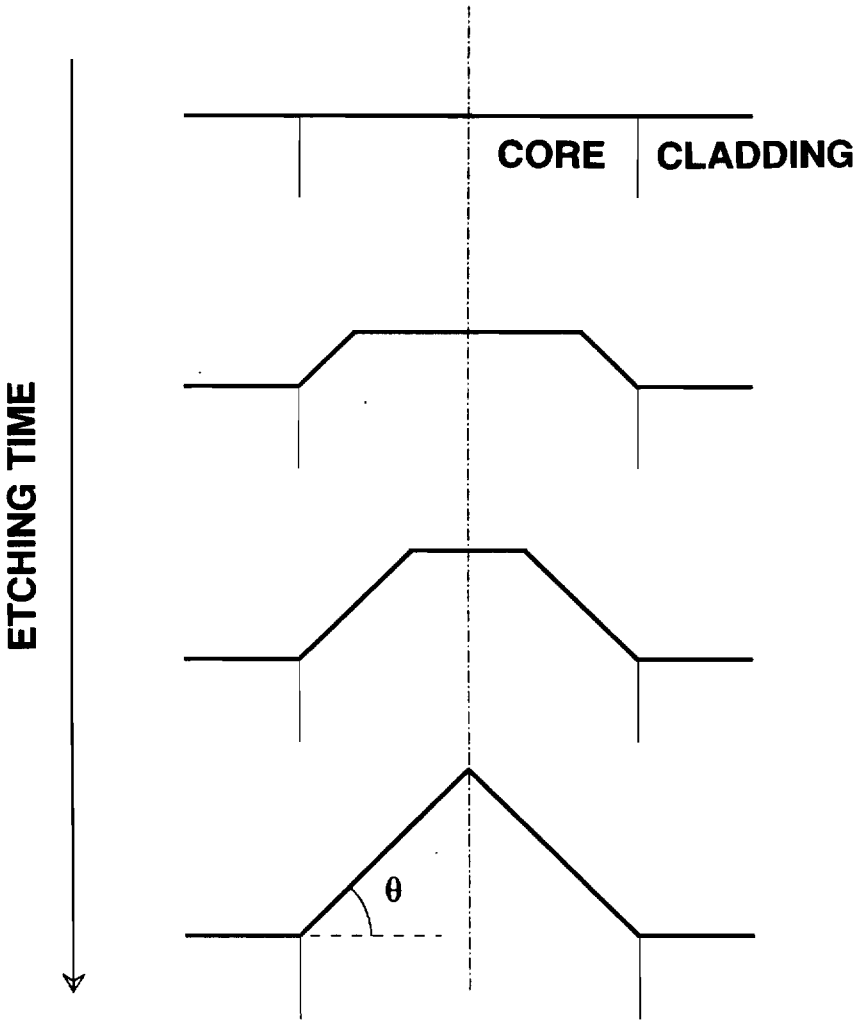

Figure 6.1 Sequential change of fiber end with chemical etching.

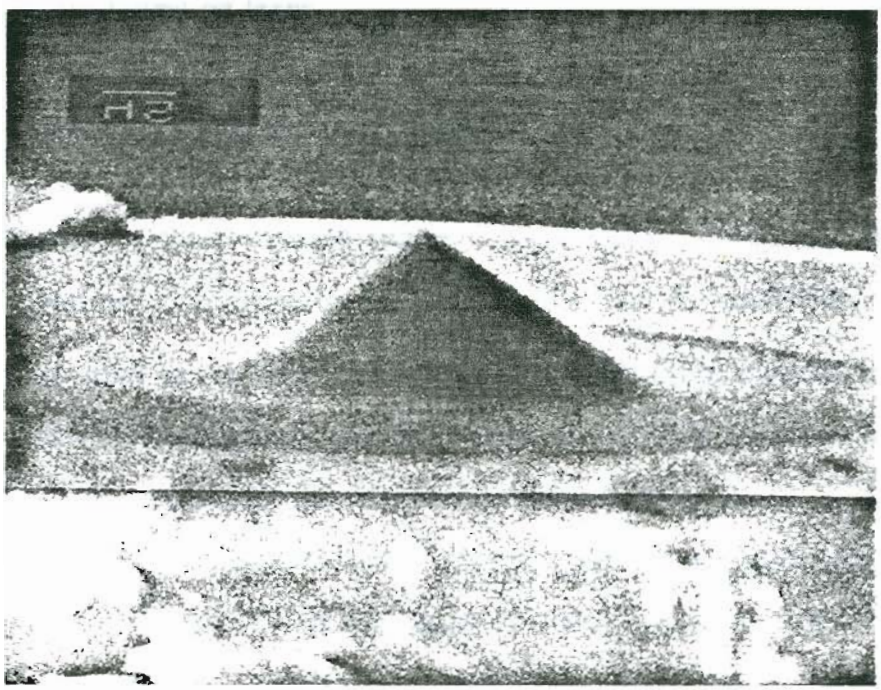

Figure 6.2 SEM micrograph of an etched conical microlens.

seconds of polishing in a air-propane flame is adequate to form such microlens structures. The microlens radius formed by the above process can be controlled by the etching time prior to fire polishing; a longer etching time gives a smaller radius. The minimum lens radius decreases with increasing GeO_2 concentration. In principle, a higher coupling efficiency is possible by coating the microlens surface with an antireflection layer.

6.2 Comparison between Theory and Experiment

In this section, the calculated values of η are compared with the experimental results obtained with, respectively, the butt fiber and the conical lens.

The laser used in the experiment is a buried heterostructure InGaAsP semiconductor laser operating at $1.3\mu m$ wavelength is used. As the beam divergence angle of the laser perpendicular to the junction plane is nearly equal to that parallel to the junction plane, the output beam cross section approaches circularity and has a full width at half maximum (FWHM) angle, $\theta_{1/2}=32°$. The spot size of the laser beam, w_{ol}, was then estimated from $\theta_{1/2}=\tan^{-1}[(2\ln 2)^{1/2}\lambda/\pi w_{ol}]$ to be $w_{ol}=0.779\mu m$.

A high-precision micromanipulator holding the fiber had a positioning resolution of $0.01\,\mu m$. The fiber and laser positions were aligned by the micromanipulator, which was driven by stepper motors in three mutually orthogonal directions. Electric micrometers were used to evaluate the effect of fiber lateral displacements and distance from the laser facet. Next, the laser was coupled into a 1 ft long fiber and the power at the output cleaved surface of the fiber was meas-

ured by a power meter. The coupling efficiency was obtained from the ratio between the power P_0 emitted from the laser and the power P_1 emitted from the 1 ft fiber, corrected for the about 8% loss due to reflections at the conical surface (5.5%) and at the cleaved surface (3.4%)[17]. The coupling loss was evaluated from the same ratio by

$$\text{Coupling loss (dB)} = -10 \log \left(\frac{P_1}{P_0} \right) + 0.35 , \qquad (6.2)$$

where 0.35 dB added is the reflection loss.

Figure 6.3 shows the comparison of the theory with the experiment using the dependence of the coupling loss on the distance between the laser surface and the tip of the conical microlens with a 2.6 μm height. The circles represent experiment values. The solid curve represents theoretical values calculated from the *ABCD* law. The stars represent theoretical values including the diffraction loss. Since it is much more complicated to directly use diffraction theory for the conical microlens, the diffraction calculation is carried out only for the hemispherical microlens. However, it is reasonable to assume that the diffraction loss could be about same for both the hemispherical and conical microlenses. Therefore, as the first order of approximation, the diffraction loss of the hemispherical microlens is used for the conical microlens. The lowest coupling loss is 2.7 dB (54% coupling efficiency) under the optimum alignment conditions. This result is 7.4 dB lower than the 10 dB loss obtained with a simple butt joint. The experimental coupling loss at the optimum position is about 0.6 dB higher than the corresponding theoretical values from the *ABCD* law. When the diffraction loss is included, the discrepancy between the theoretical and experimental values is 0.3 dB at this

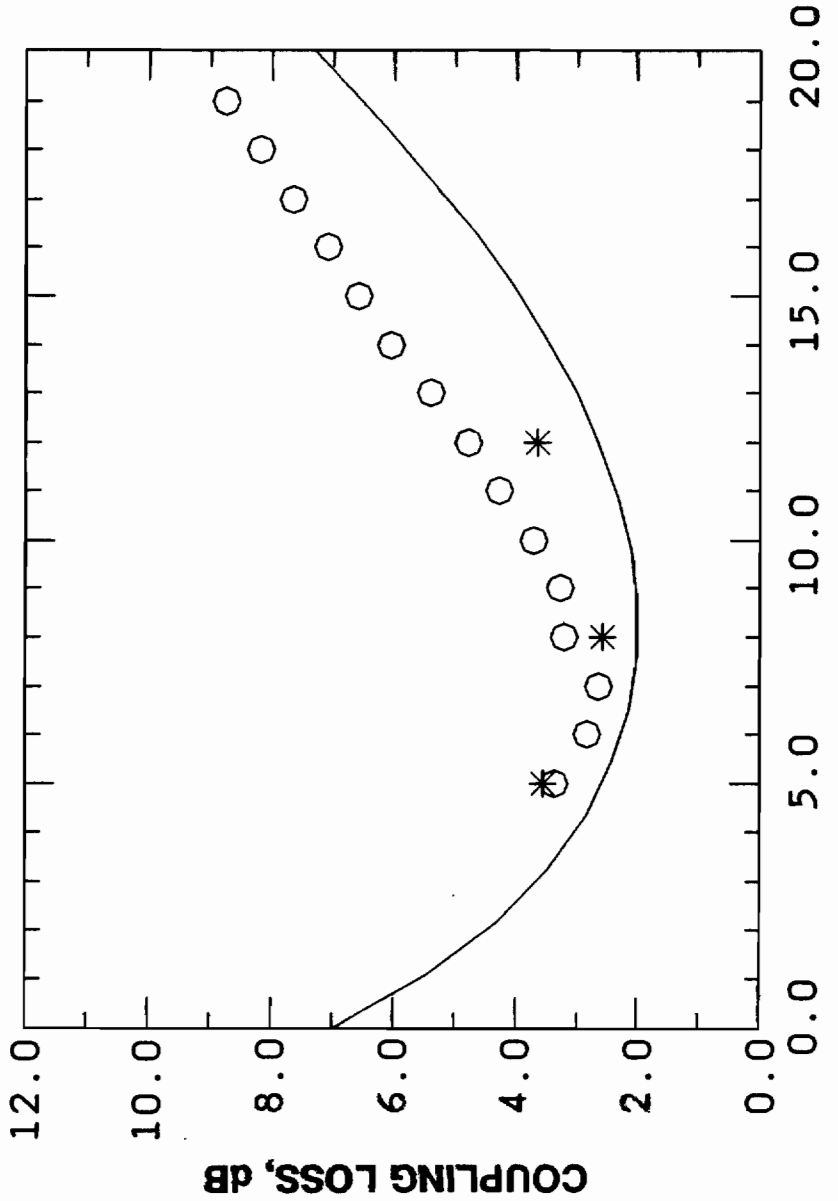

Figure 6.3 Experimental and theoretical coupling efficiency of conical lens vs laser-to-fiber distance. The beam spot size is symmetric. The circle represents experimental value, the solid line theoretical value from the *ABCD* law and the star theoretical value including the diffraction loss, respectively.

point. The overall agreement is good and the diffraction theory is slightly better.

The butt-coupling efficiency, in which the laser beam is directed into a butt fiber without any lens, was also measured for comparison. As the laser-fiber distance is varied, the coupled power oscillates with a period equal to laser half-wavelength, centered at an average value of about 10%. Figure 6.4 shows both experimentally measured data and theoretically calculated values for the butt-coupling efficiency. The oscillating behavior of η at half wavelength intervals is evidently due to the interference effect of the Fabry-Perot etalon of the air formed by the plane parallel faces of the laser and the fiber. The transmittance of this F-P etalon is given by

$$T = \frac{4nn_1}{(n_1+n)^2 - (1-n^2)(n_1-1)\sin^2(\delta/2)} \quad , \tag{6.3}$$

where n, n_1 denote the index of refraction of the laser diode and the fiber core respectively and $\delta = 4\pi d/\lambda$. Therefore, the effective coupling efficiency in this case can be obtained by multiplying the transmittance and the butt-coupling efficiency:

$$\eta_{eff} = T\eta_{butt} \quad . \tag{6.4}$$

Here, η_{butt} is a special case of conical lens with $h = 0$. Aside from the difference in absolute magnitude of η by about 25%, the general agreement between theory and experiment is satisfactory. The observed discrepancy might perhaps be due to lens imperfection, misalignment, etc. A butt fiber is particularly sensitive to angular misalignments[72], which were not controllable in the experiment.

In this work, generally in almost all the theoretical works, the calculated

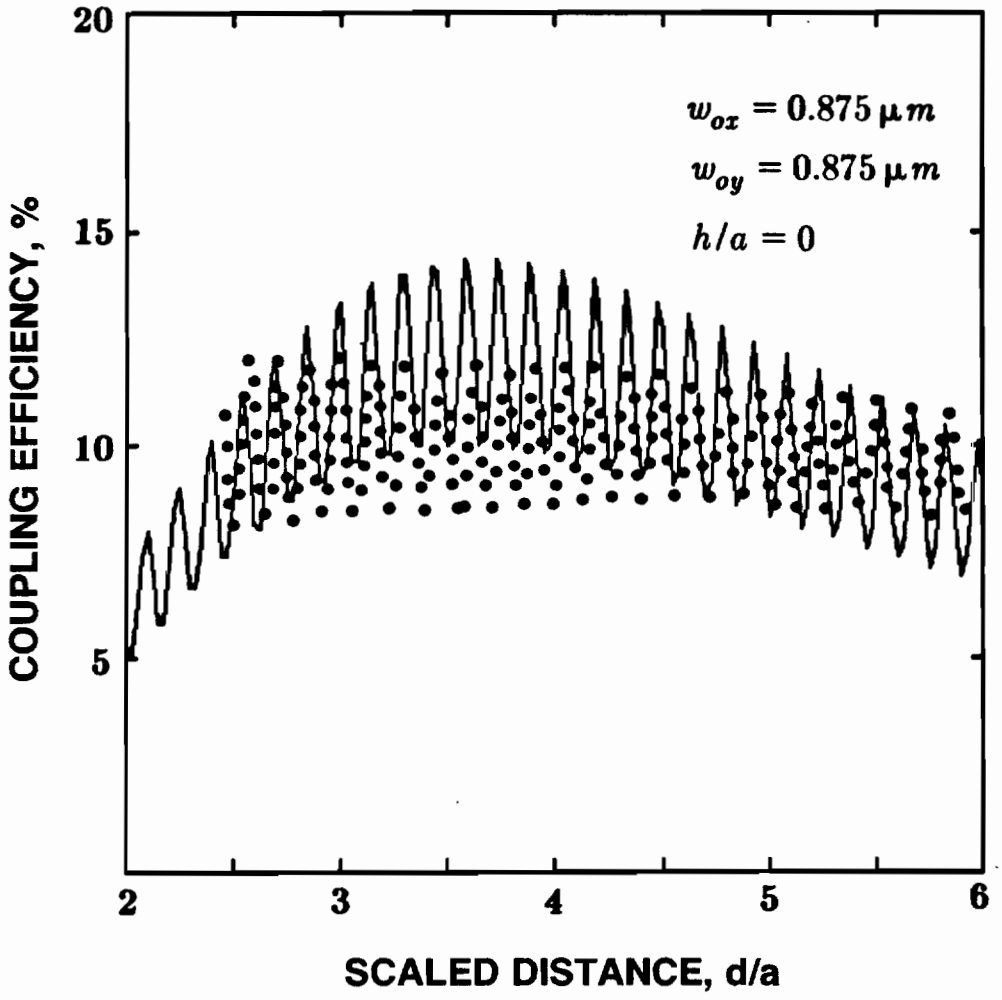

Figure 6.4 Experimental (filled dot ●) and theoretical (solid line -) coupling efficiency of butt fiber vs laser-to-fiber distance. The beam spot size is symmetric.

coupling efficiencies are higher than the actual experimental results. The discrepancy may be contributed to, in addition to the experimental imperfections, the simplified conditions used in the calculations such as ignoring the reflection and diffraction losses at the lens and the lens aberrations. The reflection fed back into the laser may also disturb the laser output properties and in turn affect the coupling efficiency, The feedback effect has been shown to be very secondary, the feedback efficiency defined as the ratio of feedback amount into the laser to the total amount emitted from the laser was found to be below -50 dB with tapered hemispherical end fibers[73]. Numerical computations also showed that for the majority of the microlenses formed on the end of single-mode fibers, the truncations and aberrations are small so that the truncated or aberrated Gaussian beam can be approximated as a Gaussian beam[74]. However, the diffraction effect becomes noticeable as the aperture of the microlens is of the same order as the beamwidth, [56] and the field will be different from that obtained using the *ABCD* law.

7. CONCLUDING REMARKS

In this thesis, the coupling efficiency of a single-mode diode laser to a single-mode optical fiber has been comprehensively analyzed. The two analytical methods based on the *ABCD* law and the diffraction theory were used to discuss the coupling problem. Naturally, using the *ABCD* law is easier and faster. However, it gives accurate results primarily for paraxial beams. If the source spot size is sufficiently small, the diffraction theory should be used. The diffraction theory is more rigorous, but the diffraction integral cannot be evaluated easily and one must resort to tedious numerical methods.

Specifically, the coupling efficiency has been systematically characterized in terms of the laser-to-fiber distance, the shapes of the laser beam and the lens used. Theoretical results thus obtained are compared with experimental data. It is shown that the theoretical coupling efficiencies obtained with the conical lens and butt fiber are in good agreement with the corresponding experimental values.

The relative figure of merits for hemispherical, conical and butt fibers are graphically summarized in Figure 7.1. Here, the coupling efficiency is plotted as a function of the laser-to-fiber distance using some typical parameters of laser diode and optical fiber. It is clear from the figure that higher coupling efficiency can be achieved with a hemispherical lens. However, the difference between the

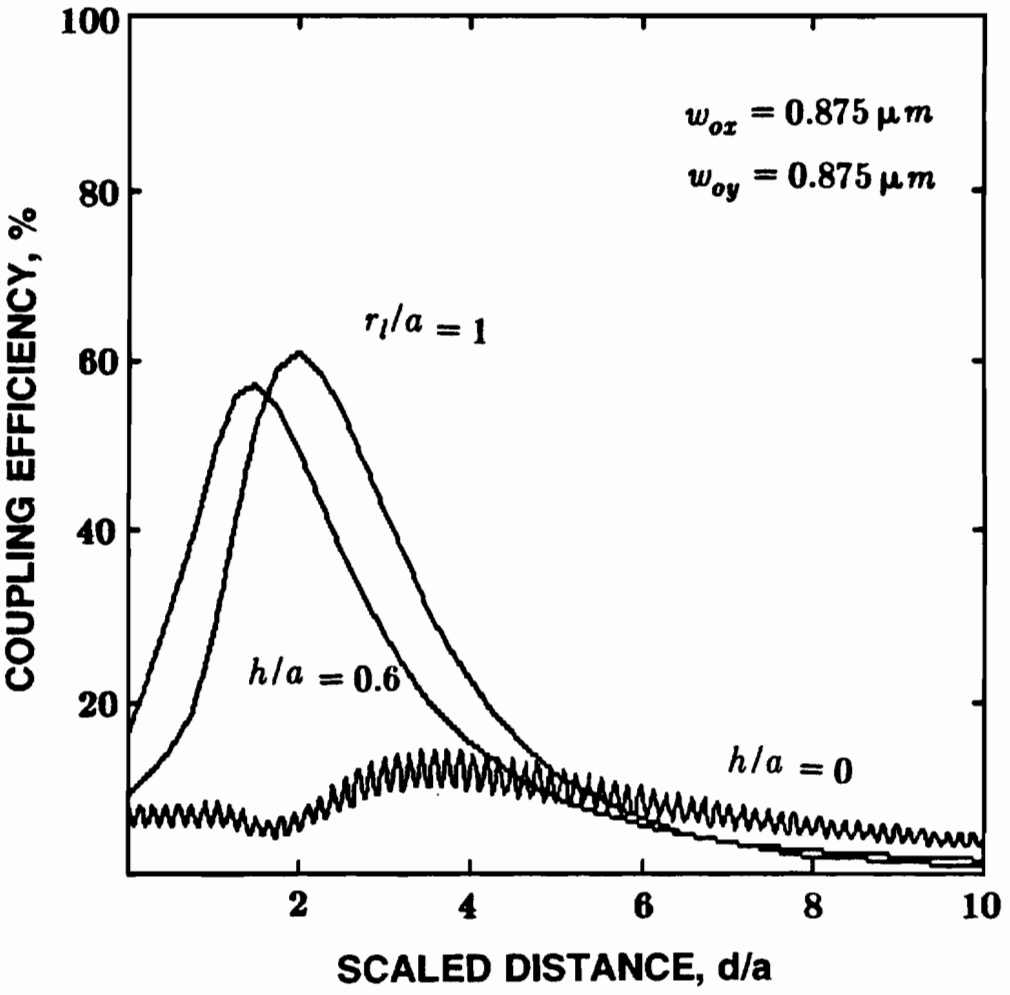

Figure 7.1 Coupling efficiencies of hemispherical (a), conical (b) and butt (c) fibers vs laser-to-fiber distance. The beam spot size was taken to be symmetric.

maximum efficiency with a hemispherical lens and that with a conical lens is not significant. This suggests that the use of the conical lens is perhaps the attractive route because of its relative simplicity of fabrication and its reproducibility.

References

1. J. I. Minowa, M. Saruwatari, and N. Suzuki, "Optical componentry utilized in field trial of single-mode fiber long-haul transmission," *IEEE J. Quantum Electron.*, vol. QE-18, pp. 705-717, Apr. 1982.
2. M. Saruwatari, K. Asatani, J. Yamada, I. Hatakeyama, K. Sugiyama, and T. Kimura, "Low loss fiber transmission of high speed pulse signals at 1.29 μm wavelength," *Electron. Lett.*, vol. 14, p. 187, March 1978.
3. T. Kimura and K. Daikoku, "A proposal on optical fibre transmission systems in a low-loss 1.0-1.4 μm wavelength region," *Opt. & Quantum Electron.*, vol. 9, pp. 33-42, 1977.
4. M. M. Boenke, R. E. Wagner, and D. J. Will, "Transmission experiments through 101 km and 84 km of single-mode fibre at 274 Mbit/s and 420 Mbit/s," *Electron. Lett.*, vol. 18, p. 897, Oct. 1982.
5. W. Albrecht, C. Baack, G. Elze, B. Enning, G. Heydt, L. Ihlenburg, G. Walf, and G. Wenke, "Optical digital high-speed transmission: General considerations and experimental results," *IEEE J. Quantum Electron.*, vol. QE-18, p. 1547, Oct. 1982.
6. J. Yamada, M. Saruwatari, K. Asatani, H. Tsuchiya, A. Kawana, K. Sugiyama, and T. Kimura, "High-speed optical pulse transmission at 1.29-μm wavelength using low-loss single-mode fibers," *IEEE J. Quantum Electron.*, vol. QE-14, pp. 791-800, Nov. 1978.
7. A. Kawana, M. Kawachi, T. Miyashita, M. Saruwatari, K. Asatani, J. Yamada, and K. Oe, "Pulse broadening in long-span single-mode fibers around a material-dispersion-free wavelength," *Opt. Lett.*, vol. 2, p. 106, Apr. 1978.
8. T. Kimuar, "Single-mode systems and components for longer wavelengths," *IEEE Transactions on Circuits and Systems*, vol. CAS-22, p. 987, Dec. 1979.
9. J. Yamada, S. Machida, T. Mukai, H. Tsuchiya, and T. Kimura, "Long-span single-mode fiber Transmission characteristics in long wavelength regions," *IEEE J. Quantum Electron.*, vol. QE-16, pp. 874-884, Aug. 1980.
10. C. J. Lilly, "The state of the art and application of optical fiber systems operating at the longer wavelength of 1300-1600 nm," *Proc. of the 8th European Conference on Optical Communication, Cannes, Frances*, pp. 17-23, Sept. 1982.
11. K. Shirahata, W. Susaki, and H. Amizaki, "Recent development on fiber optic devices," *IEEE J. Trans. Microwave Theory Tech.*, vol. MTT-30, p. 121, Feb. 1982.
12. D. E. Payne and W. A. Gambling, "Zero material dispersion in optical fibers," *Electron. Lett.*, vol. 11, pp. 176-178, 1975.
13. J. Yamada, S. Machida, and T. Kimura, "2 Gbit/s optical transmission experiments at 1.3 μm with 44 km single-mode fibre," *Electron. Lett.*, vol. 17, p. 479, June 1981.
14. H. Murata and N. Inagaki, "Low-loss single-mode fiber development and splicing research in Japan," *IEEE J. Quantum Electron.*, vol. QE-17, pp.

835-849, June 1981.

15. G. D. Khoe, H. G. Kook, D. Kuppers, J. Poulissen, and H. M. de Vrieze, "Progress in monomode optical-fiber interconnection devices," *IEEE J. Lightwave Technol.*, vol. LT-2, pp. 217-227, June 1984.
16. J. Yamada, S. Machida, T. Mukai, H. Kano, and K. Sugiyama, "Modulation characteristics of 1.3 μm buried-stripe InGaAsP laser up to 2 Gbit/s data rates," *Electron. Lett.*, vol. 15, p. 596, Sept. 1979.
17. G. Eisenstein and D. Vitello, "Chemically etched conical microlenses for coupling single-mode lasers into single-mode fibers," *Appl. Opt.*, vol. 21, pp. 3470-3474, Oct. 1982.
18. L. G. Cohen, "Power coupling from GaAs injection laser into optical fibers," *Bell Syst. Tech. J.*, vol. 51, pp. 573-594, March 1972.
19. K. Kawano, M. Saruwatari, and O. Mitomi, "A new confocal combination lens method for a laser-diode module using a single-mode fiber," *IEEE J. Lightwave Technol.*, vol. LT-3, p. 739, 1985.
20. E. Weidel, "New coupling method for GaAs-laser-fiber coupling," *Electron. Lett.*, vol. 11, pp. 436-437, Sept. 1975.
21. K. Nishizawa and H. Nishi, "Coupling characteristics of gradient-index lenses," *Appl. Opt.*, vol. 23, pp. 1711-1714, June 1984.
22. J. M. Stagaman and D. T. Moore, "Laser diode to fiber coupling using anamorphic gradient-index lenses," *Appl. Opt.*, vol. 23, pp. 1730-1734, June 1984.
23. A. Nicia, "Lens coupling in fiber-optic devices: efficiency limits," *Appl. Opt.*, vol. 20, pp. 3136-3145, Sept. 1981.
24. M. Sumida and K. Takemoto, "Lens coupling of laser diodes to single-mode fibers," *IEEE J. Lightwave Technol.*, vol. LT-2, pp. 305-311, June 1984.
25. M. Saruwatari and K. Nawata, "Semiconductor laser to single-mode fiber coupler," *Appl. Opt.*, vol. 18, pp. 1847-1856, June 1979.
26. H. Honmou, R. Ishikawa, H. Ueno, and M. Kobayashi, "1.0 dB low-loss coupling of laser diode to single-mode fibre using a planoconvex graded-index rod lens," *Electron. Lett.*, vol. 22, p. 1122, Oct. 1986.
27. M. Saruwatari and T. Sugie, "Efficient laser diode to single-mode fiber coupling using a combination of two lenses in confocal condition," *IEEE J. Quantum Electron.*, vol. QE-17, pp. 1021-1027, June 1981.
28. M. Saruwatari and T. Sugie, "Efficient laser-diode-single-mode-fiber coupling using two confocal lenses," *Electron. Lett.*, vol. 16, p. 955, Dec. 1980.
29. L. A. Reith, P. W. Shumate, and Y. Koga, "Laser coupling to single-mode fiber using graded-index lenses and compact disc 1.3 μm laser package," *Electron. Lett.*, vol. 22, pp. 836-838, July 1986.
30. K. Kawano and O. Mitomi, "Coupling characteristics of laser diode to multimode fiber using separate-lens methods," *Appl. Opt.*, vol. 25, p. 2600, Jan. 1986.

31. D. Kato, "Light coupling from a stripe-geometry GaAs diode laser into an optical fiber with spherical end," *J. Appl. Phys.*, vol. 44, pp. 2756-2758, June 1973.

32. L. G. Cohen and M. V. Schneider, "Microlenses for coupling optical fibers to junction lasers," *J. Opt. Soc. Am.*, vol. 63, p. 1294, 1973.

33. E. Weidel, "Light coupling from a junction laser into a monomode fibre with a glass cylindrical lens on the fibre end," *Opt. Commun.*, vol. 12, pp. 93-97, Sept. 1974.

34. C. C. Timmermann, "Highly efficient light coupling from GaAlAs lasers into fibers," *Appl. Opt.*, vol. 15, pp. 2432-2433, Oct. 1976.

35. L. G. Cohen and M. V. Schneider, "Microlenses for coupling junction lasers to optical fibers," *Appl. Opt.*, vol. 13, pp. 89-94, Jan. 1974.

36. H. Ghafoori-shiraz and T. Asano, "Microlens for coupling a semiconductor laser to a single-mode fiber," *Opt. Lett.*, vol. 11, pp. 537-529, Aug. 1986.

37. Y. Murakami, J. Yamada, J. Sakai, and T. Kimura, "Microlens tipped on a single-mode fiber end for InGaAsP laser coupling improvement," *Electron. Lett.*, vol. 16, pp. 321-322, Apr. 1980.

38. J. Yamada, Y. Murakami, J. Sakai, and T. Kimura, "Characteristics of a hemispherical microlens for coupling between a semiconductor laser and single-mode fiber," *IEEE J. Quantum Electron.*, vol. QE-16, pp. 1067-1072, Oct. 1980.

39. W. Bludau and R. H. Rossberg, "Low-loss laser-to-fiber coupling with negligible optical feedback," *IEEE J. Lightwave Technol.*, vol. LT-3, pp. 294-302, Apr. 1985.

40. H. Kuwahara, M. Sasaki, and N. Tokogo, "Efficient coupling from semiconductor lasers into single-mode fibers with tapered hemispherical ends," *Appl. Opt.*, vol. 19, pp. 2578-2583, Aug. 1980.

41. P. Kayoun, C. Puech, M. Papuchon, and H. J. Arditty, "Improved coupling between laser diode and single-mode fiber tipped with a chemically etched self-centred diffracting element," *Electron. Lett.*, vol. 17, p. 400, June 1981.

42. A. Yariv and P. Yeh, *Optical Wave in Crystals*, John Wiley & Sons, New York, 1984.

43. T. H. Zachos, "Gaussian beams from GaAs junction lasers," *Appl. Phys. Letters*, vol. 12, pp. 318-320, May 1968.

44. T. H. Zachos and J. C. Dyment, "Resonant mode of GaAs junction lasers — III: Propagation characteristics of laser beams with rectangular symmetry," *IEEE J. Quantum Electron.*, vol. QE-6, pp. 317-324, June 1970.

45. I. P. Kaminow, G. Eisenstein, L. W. Stulz, and A. G. Dentai, "Lateral confinement InGaAsP superluminescent diode at 1.3 micron," *IEEE J. Quantum Electron.*, vol. QE-19, pp. 78-82, Jan. 1983.

46. D. Marcuse, *Light Transmission Optics*, Van Nostrand Reinhold, New York, 1982. Second Edition

47. D. D. Cook and F. R. Nash, "Gain-induced guiding and astigmatic output beam of GaAs lasers," *J. Appl. Phys.*, vol. 46, pp. 1660-1672, Apr. 1975.

48. K. Tatsuno and A. Arimoto, "Measurement and analysis of diode laser wave fronts," *Appl. Opt.*, vol. 20, pp. 3520-3525, Oct. 1981.

49. T. P. Lee, C. A. Burrus, D. Marcuse, and A. G. Dentai, "Measurement of beam parameters of index-guided and gain-guided single-frequency InGaAsP Injection lasers," *Electron. Lett.*, vol. 18, pp. 902-904, Oct. 1982.

50. H. Kogelnik, "On the propagation of Gaussian beam of light through lens-like media including those with a loss or gain variation," *Appl. Opt.*, vol. 4, p. 1562, 1965.

51. A. Gerrard and J. M. Burch, Introduction to Matrix Methods in Optics, John Wiley & Sons, London, 1975.

52. A. Yariv, *Optical Electronics*, Holt, Rinehart and Winston, New York, 1985. Third Edition

53. D. Marcuse, "Loss analysis of single-mode fiber splices," *Bell. Syst. Tech. J.*, vol. 56, pp. 703-718, May-June 1977.

54. H. Kogelnik, "Coupling and Conversion coefficients for optical modes," *Proc. Symposium on Quasi-Optics*, pp. 333-347, Polytechnic Press, New York, 1964.

55. R. G. Hunsperger, *Integrated Optics: Theory and Technology*, pp. 88-106, Springer-Verlag, New York, 1985.

56. K. Tanaka, M. Shibukawa, and O. Fukumitsu, *IEEE J. Trans. Microwave Theory Tech.*, vol. MTT-20, p. 749, 1972.

57. H. Kogelnik, "Imaging of Optical Modes — Resonators with Internal Lenses," *Bell Syst. Tech. J.*, vol. 44, p. 455, 1965.

58. N. Saga, K. Tanaka, and O. Fukumitsu, "Diffraction of a Gaussian beam through a finite aperture lens and the resulting heterodyne efficiency," *Appl. Opt.*, vol. 20, p. 2827, Aug. 1981.

59. F. W. Byron and R. W. Fuller, *Mathematics of Classical and Quantum Physics*, Addison-Wesley, Reading, Massachusetts, 1970. Volume Two

60. J. M. Cowley, *Diffraction Physics*, North-Holland, Amsterdam, 1984. Second Edition

61. H. A. Haus, *Waves and Fields in Optoelectronics*, Prentice-Hall, New York, 1984.

62. J. D. Jackson, *Classical Electrodynamics*, John Wiley & Sons, New York, 1975. Second Edition

63. J. A. Arnaud, *Beam and Fiber Optics*, Academic Press, New York, 1976.

64. A. E. Siegman, *Lasers*, University Science Books, Mill Vally, California, 1986.

65. M. Born and E. Wolf, *Principles of Optics*, Pergamon Press, New York, 1975. Fifth Edition

66. P. M. Morse and H. Feshbach, *Methods of Theoretical Physics*, McGraw-Hill, New York, 1953. Part I

67. J. W. Gibbs, *Vector Analysis*, Dover Publications, New York, 1960.

68. T. N. L. Patterson, "The optimum addition of points to quadrature formulae," *Math. Comp.*, vol. 22, pp. 847-856, 1968.

69. P. D. Bear, "Microlenses for coupling single-mode to single-mode thin-film waveguides," *Appl. Opt.*, vol. 19, pp. 2906-2909, Sept. 1980.

70. M. L. Dakss and B. Kim, "Simple self-centring technique for mounting microsphere coupling lens on a fibre," *Electron. Lett.*, vol. 16, pp. 463-464, June 1980.

71. M. Kawachi, T. Edahira, and H. Toba, "Microlens formation on VAD single-mode fibre ends," *Electron. Lett.*, vol. 18, p. 71, Jan. 1982.

72. W. B. Joyce and B. C. Deloach, "Alignment of Gaussian beams," *Appl. Opt.*, vol. 23, pp. 4187-4196, Dec. 1, 1984.

73. H. Kuwahara, Y. Onoda, M. Goto, and T. Nakagami, "Reflected light in the coupling of semiconductor lasers with tapered hemispherical end fibers," *Appl. Opt.*, vol. 22, p. 2732, Sept. 1983.

74. K. S. Lee, "Focusing characteristics of a truncated and aberrated Gaussian beam through a hemispherical microlens," *Appl. Opt.*, vol. 25, pp. 3671-3676, Oct. 1986.

BIOGRAPHICAL NOTE

The author was born in Sichuan, China on April 2, 1958. He attended Huazhong University of Science and Technology in Wuhan, China, and received the Bachelor of Science degree in Optical Engineering in January 1982. From 1982 through 1984, he worked as a research assistant at Wuhan Institute of Physics, Academia Sinica, China.

The author began his studies at the Oregon Graduate Center in January 1985 and completed the requirements for the degree Master of Science in Electrical Engineering in February 1987.

The author has been married since 1982 to the former Yuan Liu.